Crystallographic and Computational Analysis of Solid Form Landscape of Three Structurally Related Imidazolidine-2,4-dione Active Pharmaceutical Ingredients: Nitrofurantoin, Furazidin and Dantrolene

Aija Trimdale-Deksne[1], Artis Kons[1], Liāna Orola[1], Anatoly Mishnev[2], Dmitrijs Stepanovs[2], Liliana Mazur[3], Magdalena Skiba[3], Marta K. Dudek[4], Nicolas Fantozzi[5], David Virieux[5], Evelina Colacino[5], Agris Bērziņš[1]**

[1]Faculty of Chemistry, University of Latvia, Jelgavas iela 1, LV-1004, Riga, Latvia.

[2]Latvian Institute of Organic Synthesis, Aizkraukles iela 21, LV-1006 Riga, Latvia.

[3]Institute of Chemical Sciences, Faculty of Chemistry, Maria Curie-Skłodowska University, Maria Curie-Skłodowska Square 2, 20-031 Lublin, Poland

[4]Polish Academy of Sciences, Centre of Molecular and Macromolecular Studies, 90-363 Lodz, Poland

[5]ICGM, Univ Montpellier, CNRS, ENSCM, Montpellier 34296, France

ABSTRACT

We present a crystallographic and computational study of three hydantoin-based active pharmaceutical ingredients nitrofurantoin, furazidin, and dantrolene aimed at identifying factors resulting in different propensities of these compounds to form polymorphs, hydrates, solvates, and solvate hydrates. This study is a continuation of our research towards understanding how small structural differences in closely related compounds affect their propensity to form different crystal

phases, as all three compounds contain an imidazolidine-2,4-dione scaffold and a *N*-acyl hydrazone moiety and all form multiple crystalline phases. Crystallographic and computational analysis of the already known and newly obtained nitrofurantoin, furazidin and dantrolene crystal structures was performed by dissecting the properties of individual molecules and searching for the differences in tendency to form hydrogen bonding patterns and characteristic packing features. The propensity to form solvates was found to correlate with the relative packing efficiency of neat polymorphs and solvates and the ability of molecules to pack efficiently in several different ways. Additionally, the differences in propensity to form solvate-hydrates were attributed to the different stability of the hydrate phases.

1 INTRODUCTION

When crystallized from a solution, many organic compounds can form multiple solid phases – solvent-free (including polymorphs) or multiple component phases such as hydrates, solvates, salts, co-crystals and other phases [1]. A recent survey[2] on organic solvates deposited in the Cambridge Structural Database (CSD) categorized 325 104 unique organic structures. Of these, 83.8% were solvent-free phases (including multi-component crystals), 8.3% were single-organic solvent solvates, 6.4% were hydrates, and only 1.5 % of the structures contained at least two solvents, including solvate-hydrates (1.1 %) and heterosolvates (0.4 %).

Studies on solvate, solvate-hydrate and hydrate formation, occurrence and crystal structure analysis have been conducted on compounds having rich solid-form landscape, for example, prolific solvate formers olanzapine[3], galunisertib[4], axitinib[5] and sulfathiazole[6] as well as solvate-hydrate formers such as bosutinib[7] and 3,5-dihydroxybenzoic acid[8,9]. The formation of multiple crystalline phases represents a possible strategy for altering the solid-state properties of pharmaceutical compounds, influencing the physicochemical and biopharmaceutical properties (*e.g.* the dissolution rate profile and hence, bioavailability) without affecting the physiological action.[10,11] Therefore, considering the importance of solid crystalline forms and solvates in the pharmaceutical industry[12] and their implication in the pharmaceutical development of small organic drug molecules,[13] the large number of characterized solid forms for pharmaceutical compounds is not surprising.

Currently, general observations from such studies allow to conclude that the two main driving forces for formation of solvated crystalline phases of a substance are a) formation of host–guest interactions, typically strong hydrogen bonds, and b) solvent provided additional lattice stabilization via weak intramolecular interactions, decreased void space and improved crystal packing efficiency. Most solvates include contributions from both driving forces[14–18]. In the previous papers, authors have used different combinations of various methods, *e.g.* experimental solid-form landscape screening, experimental evaluation of the stability of various solvates, crystal structure prediction of neat polymorphs, hydrogen bond network analysis in crystal structures, lattice energy, conformational energy and packing efficiency calculations, molecular conformation, electrostatic potential (ESP), Hirshfeld surface analysis and other methods.

Although previous studies contribute towards the understanding of the factors influencing the formation and diversity of solvates, the above-mentioned studies analyse multiple solvated phases formed by a single organic compound. To determine the possible causes of differences in solvate formation between similar compounds, in our previous studies[19–21] we have already compared structurally similar compounds of pharmaceutical interest by investigating how small structural differences between these compounds affect their propensity to form different solvent-free and solvated crystal phases. We have identified that altered formation of weak intermolecular interactions[19] or intramolecular hydrogen bonding [20], as well as a higher abundance of associates in solution[20] and an increased packing efficiency[21] are factors that contribute to an increased propensity to form solvates among structurally similar compounds.

In this study, we continued our research toward rationalizing trends related to the occurrence of solvated and hydrated crystalline phases by studying three hydantoin–based marketed drugs:[22,23] the essential medicine of the World Health Organization (WHO), the urinary track antibiotic nitrofurantoin (NF)[24], its structural analogue furazidin (FUR) and muscle relaxant dantrolene (DAN)[25] (Figure 1). Structurally similar, they contain an imidazolidine-2,4-dione scaffold and a *N*-acyl hydrazone moiety and are characterised by a very poor water solubility. They form various crystalline phases, and part of their solvates, hydrates and solvate-hydrates are well-characterized. Here we present crystallographic and computational analysis of 13 nitrofurantoin crystal structures (2 polymorphs, 2 hydrates, 9 solvates), 14 furazidin crystal structures (3 polymorphs, 7 solvates and 4 solvate-hydrates) and 21 dantrolene crystal structures (6 polymorphs, 4 hydrates, 10 solvates and 1 solvate-hydrate), by dissecting properties of individual molecules and searching for the tendency to form hydrogen bonding patterns in an attempt to contribute to the understanding of the impact of small structural changes on the differences in crystal phase formation.

2 EXPERIMENTAL SECTION

Materials. Nitrofurantoin (purity >98%) was purchased from Alfa Aesar. Dantrolene and furazidin (purity >99%) were obtained from JSC Olainfarm (Olaine, Latvia). The dantrolene batches used for the preparation of DMF, DMSO and 1,4-dioxane solvates as well as single crystals of Dan II were obtained mechanochemically according to the procedure described in the literature[26] (more details in the Supporting Information). Organic solvents of analytical grade were purchased from commercial sources and used without further purification.

Crystalline phase preparation. Nitrofurantoin and dantrolene solvates were prepared by cooling to room temperature a hot concentrated solution in the selected solvent or by evaporation of a saturated solution at ambient temperature. Both methods produced 10 dantrolene solvates with ethanol, nitromethane, dimethyl carbonate, 1,3-dioxolane, DMSO, DMF, 1,4-dioxane and tetrahydrofuran/water (good quality single crystals were obtained) as well as acetonitrile and formic acid (in a form of polycrystalline powder). Crystallization of a mechanochemically obtained dantrolene[26] from acetone produced single crystals of the polymorph DAN II. For nitrofurantoin, we obtained 4 solvates with 2-propanol, benzyl alcohol, *tert*-butanol and cyclohexanol (all in a form of very small crystals or polycrystalline powder). The monohydrate

DAN H IV was prepared by hydrating dantrolene nitromethane solvate DAN S_{NM} in a desiccator at 25 °C over saturated K_2SO_4 solution (97% relative humidity). Furazidin polymorphs FUR I and FUR II were prepared by crystallization from acetonitrile and acetone respectively. FUR III was obtained in crystallization from acidified acetone solution.

Structure determination from X-ray powder diffraction (XRPD) data. XRPD data for crystal structure determination were recorded at ambient temperature on a Bruker D8 Discover diffractometer using Cu Kα radiation (λ = 1.54180 Å), equipped with LynxEye (1D) detector in transmission mode. Tube voltage and current were set to 40 kV and 40 mA. The sample was loaded into a special glass No.10 capillary (0.5 mm in diameter). A capillary spinner (60 rpm) and upper and lower knife edges were used. The diffractometer incident beam path was equipped with a Göbel mirror, a Soller slit, and a 0.6 mm divergence slit, the diffracted beam path was equipped only with a Soller slit. The diffraction patterns were recorded on the 2θ scale from 3° or 4.5° to 70° at a step size of 0.01° using a scan speed of 36 s per step.

Indexing, determination of space groups and structure solution were performed using EXPO2014[27]. Unit cell dimensions were determined by applying the N-TREOR09[28] and Dicvol06[29] indexing procedures with a set of 20–25 reflections found in 4.5–30° 2θ range. The determination of the space group was carried out using a statistical assessment of systematic absences, and Z′ was determined based on density considerations. The cell and diffraction pattern profile parameters were refined according to the Le Bail algorithm[30]. The background was modelled by a 20th-order polynomial function of the Chebyshev type, peak profiles were described by the Pearson VII function. The initial geometry of nitrofurantoin was taken from polymorph NF β[31], and of dantrolene was taken from methanol solvate DAN S_{MeOH}[32]. Simulating Annealing algorithm was used to optimize the model against the experimental powder diffraction pattern set in direct space by adjusting the conformation, position, and orientation of the trial model in the unit cell. The best structure solution was then used for the Rietveld refinement using TOPAS5[33]. The background was modelled with Chebyshev polynomials, the modified Thompson-Cox-Hastings pseudo-Voigt function was used for peak shape fitting. The geometry of each molecule was defined by a rigid body. Rotation and translation parameters were refined simultaneously with the dihedrals of each independent molecule in the asymmetric unit. A global isotropic atomic displacement parameter (B_{iso}) was refined for non-hydrogen atoms, and for hydrogen atoms it was set to 1.2 B_{iso}.

Single-crystal X-ray diffraction. SCXRD data for the solvates, excluding DAN S_{DXN}, S_{DMF} and S_{DMSO}, were collected on a XtaLAB Synergy-S Dualflex diffractometer (RIGAKU Oxford Diffraction) equipped with a HyPix6000 detector and a microfocus sealed X-ray tube with Mo Kα radiation (λ = 0.7107 Å). A single crystal with dimensions of $<0.1 \times <0.1 \times <0.1$ mm^3 was fixed with oil in a nylon loop of a magnetic CryoCap and set on a goniometer head. The sample was cooled to 150 – 170 K, and ω scans were performed with a step size of 0.5°. Data collection and reduction were performed with the CrysAlisPro 1.171.40.35a software. Structure solution and refinement were performed with AutoChem3.0 and SHELXL[34] software that are parts of the CrysAlisPro suite. Non-hydrogen atoms were refined anisotropically. Hydrogen atoms were added geometrically and refined using a 'riding' model.

SCXRD data for FUR polymorphs were measured with a Nonius Kappa CCD diffractometer (Bruker AXS) with Mo Kα radiation (λ = 0.71073 Å). Data were collected at 190 K. Data reduction was performed with the DENZO/SCALEPACK. Crystal structures were solved by direct methods with SHELXS-97, refinement was performed by SHELXL-97[35].

SCXRD data for DAN solvates S_{DXN}, S_{DMF} and S_{DMSO} were collected on an Oxford Diffraction SuperNova CCD diffractometer equipped with the microfocus X-ray source (Cu Kα, λ = 1.54184 Å). Single-crystal X-ray measurements on DAN II were performed using a Rigaku XtaLAB MM7HFMR diffractometer equipped with the 'quarter-chi single' goniometer, the rotating anode generator (graphite monochromated Cu Kα radiation), and the Pilatus 200K detector. In all measurements the CrysAlis^{Pro} 1.171.40.45a program was used for data collection, cell refinement and data reduction (Rigaku Oxford Diffraction, 2019)[36]. The intensities were corrected for Lorentz and polarization effects. A multi-scan absorption correction was applied. The structures were solved using the direct methods implemented in the *SHELXS-97,* and refined with the *SHELXL-18/3* program[34], both operating under *WinGX* [37]. All non-H atoms were refined with anisotropic displacement parameters. Hydrogen atoms attached to imidazolidine N1 atoms were found in the difference Fourier maps and refined with the isotropic displacement parameters. All remaining H-atoms were positioned geometrically and refined using the riding model with $U_{iso}(H) = 1.2U_{eq}$ (CH and CH_2) or $U_{iso}(H) = 1.5U_{eq}$ (CH_3).

Ab initio calculations. For electrostatic potential (ESP), initial molecular geometries were taken from crystal structures of NF α (NF conformer A), NF $S_{0.5DMSO}$ (NF conformer B), FUR II (FUR conformer A), FUR I (FUR conformer B), DAN S_{DXN} (DAN conformer A) and DAN I (DAN conformer B). Structure optimization in the gas phase was carried out in Gaussian 09[38] with the density functional theory (DFT) functional B97D and 6-31++G(d,p) basis set with the temperature and pressure fixed at the values of 298 K and 1 atm[39]. A natural bond orbital (NBO) analysis was performed using M06-2X functional with aug-cc-pVDZ base set. Further quantitative analysis of the molecular ESP surface and surface extrema was carried out in Multiwfn 3.7[40] using a spacing of grid points of 0.15 Bohr. The obtained ESP surfaces and their extrema were visualized in VMD 1.9.3[41].

Gibbs free energy values of conformers A and B of NF, FUR and DAN were calculated in Gaussian 09. The initial optimization of the conformer structure in the gas-phase was performed with the DFT functional B3LYP and 6-31G(d) basis set. Further structures were optimized and vibrational, rotational and translational frequency contributions to the free energy were calculated using M06-2X functional and 6-31++G(d,p) basis set with the temperature and pressure fixed at the values of 298 K and 1 atm[39]. More accurate electronic energies were derived from a single-point energy calculation with the aug-cc-pVDZ basis set in the gas phase and in solvent media using the SMD solvation model.

Crystal Structure Comparison and Analysis. Prior to other calculations, all used NF, FUR and DAN crystal structures were geometry optimized using Quantum ESPRESSO[42] by relaxing positions of all atoms. All calculations were performed using the PBE functional using ultra-soft pseudopotentials from the original pseudopotential library and a 44 Ry plane-wave cut-off energy with vdW interactions treated according to the D2 method of Grimme[43]. The selection of

pseudopotentials, as well as parameters of convergence and the k-point grid , was carried out using the already published suggestions for structure optimizations of pharmaceutical molecules[44].

Strong hydrogen bonds were identified and the packing coefficients were calculated in PLATON[45]. Mercury 2020.2.0[46] was used for visual crystal structure analysis. Pairwise intermolecular interaction energy calculations of crystal structures were performed in CrystalExplorer 17.5 at the B3LYP-D2/6-31G(d,p) level[47]. The sum of all pairwise interaction energies with molecules for which the atoms are within 15 Å of the central molecule was used to estimate the lattice energy of the polymorphs. CrystalExplorer 17.5 was also used for generation of energy frameworks from the calculated pairwise interaction energies and their electrostatic and dispersion components [47].

Crystal Structure Prediction (CSP). The CSP of NF polymorphs was performed with CrystalPredictor 2.2[48] using the two most likely conformers A and B (see further) as rigid entities. The other torsion angles were as in the determined experimental crystal structures. The conformational energy difference, $\Delta E_{intra,}$ was calculated with Gaussian 09[38] at the M06-2X/6-31G(d,p) level of theory and combined with the dominant intermolecular energy U_{inter} calculated as a sum of an electrostatic component derived from point charges and a repulsion-dispersion component derived from the empirically fitted FIT potential[49]. Crystal structures were generated in the 61 most common space groups in the CSD with Z' = 1 by generating a total of 500,000 structures for each conformer. After structure prediction, the obtained structures were analysed using Analysis tool, and those having reasonable lattice energy and no obvious errors were optimized in DMACRYS[50] using FIT potential and multipoles generated with GDMA[51] after M06-2X/6-31G(d,p) calculation in Gaussian 09.

The structures were then clustered, and 2017 unique structures were refined using CrystalOptimizer 2.4.7[52]. The intermolecular lattice energy was calculated using DMACRYS modelling electrostatic interactions with distributed multipoles calculated by GDMA on charge densities of isolated molecules calculated in Gaussian 09. Other intermolecular forces were calculated with an atom–atom *exp*-6 repulsion-dispersion potential using the empirically fitted FIT parameters. The conformational energies and distributed multipoles used were calculated at the M06-2X/6-31G(d,p) level. During the CrystalOptimizer optimizations torsion angles C1-N2-N3-C8 and O3-C7-C8-N3 as well as bond angle C1-N1-H were optimized. After CrystalOptimizer, structures which showed a negative eigenvalue (corresponding to a high symmetry saddle point) were re-minimized in a lower symmetry space group. The optimized structures were then clustered to obtain the final set of unique predicted crystal structures.

Analysis of computationally generated DAN and FUR crystal structures was also performed by using structures obtained in an identical CSP procedure for DAN[53] (the structures obtained after CrystalOptimizer run were used) and a similar CSP procedure for FUR[54] (the structures obtained after DMACRYS run were used).

3 RESULTS AND DISCUSSION

3.1 Complementation of solid form landscapes of the studied compounds

For nitrofurantoin, crystal structures of 2 polymorphs (NF α and NF β)[31], 2 hydrates (metastable NF HI and stable NF H II) [55] and 7 solvates (three DMA solvates labelled here as NF S_{DMA} I[56], NF S_{DMA} II[56], and NF S_{DMA} III[56], see Table S1; DMSO solvates NF S_{DMSO}[56] and NF $S_{0.5DMSO}$[56] as well as DMF solvate NF S_{DMF} [57] and methanol solvate NF S_{MeOH} [58]) were previously reported. Here we report crystal structures of 2 new NF solvates with 2-propanol NF S_{IPA} and benzyl alcohol NF S_{BnOH}. We also note that the determination of crystal structures of *tert*-butanol and cyclohexanol solvates was also attempted. Unfortunately, the obtained crystals were not of a quality for SCXRD measurements, and the XRPD data obtained from these unstable solvates were not suitable for crystal structure determination.

For furazidin crystal structures of 2 polymorphs (FUR I and FUR II determined from a crystal structure prediction study with the final structures obtained by the Rietveld refinement against the experimental XRPD patterns)[54], 7 solvates (FUR S_{DMA}[59], FUR S_{DMF}[59], FUR S_{DMSO} I[59], FUR S_{DMSO} II[59], FUR S_{DMSO} III[59], FUR S_{DXN}[59], FUR S_{HCOOH}[59]) and 4 solvate-hydrates (FUR S_{DMF} MH[60], FUR S_{THF} MH[60], FUR S_{DXN} MH[59] and FUR S_{HCOOH} MH[59]) were previously reported. Here we report and use crystal structures of FUR polymorphs I and II as well as a new polymorph III determined from SCXRD experiments.

For dantrolene, crystal structures of 6 polymorphs[53], 3 hydrates[53] (DAN H I, DAN H II, DAN H III) and 1 solvate[32] were previously reported. Additionally, the existence and crystal lattice information of numerous other solvates has also been reported[53]. Here we report crystal structures for 9 of these solvates and 1 of the solvate-hydrates, as well as a new monohydrate IV.

Basic crystallographic information of the newly determined crystal structures is summarized in Tables 1 and 2 and more details and discussion are given in the following sections. For a full list of the analysed NF, FUR and DAN crystal structures and their corresponding CSD refcodes or deposition numbers see Table S1, Supporting Information.

Table 1. Crystallographic data for the newly determined NF and DAN crystal structures obtained from XRPD data.

	NF S_{IPA}	NF S_{BnOH}	DAN S_{ACN}	DAN S_{HCOOH}	DAN H IV
Chemical formula	$C_{11}H_{14}N_4O_6$	$C_{15}H_{14}N_4O_6$	$C_{16}H_{13}N_5O_5$	$C_{15}H_{12}N_4O_7$	$C_{14}H_{12}N_4O_6$
Formula weight, g mol^{-1}	298.26	346.30	355.31	360.29	332.28
Temperature, K	293(2)	293(2)	293(2)	293(2)	293(2)
Crystal system	Monoclinic	Orthorhombic	Orthorhombic	Triclinic	Monoclinic
Space group	$P2_1/c$	$Pca2_1$	$P2_12_12_1$	$P\bar{1}$	$P2_1/c$
a, Å	18.03(2)	8.806(12)	4.8131(10)	8.142(2)	23.362(9)
b, Å	6.202(7)	6.416(9)	9.312(2)	8.844(2)	13.081(5)
c, Å	12.862(15)	28.35(4)	38.090(10)	11.410(3)	10.092(4)
α, °	90	90	90	93.581(2)	90
β, °	98.363(3)	90	90	94.801(2)	100.467(3
γ, °	90	90	90	105.504(2)	90
V, $Å^3$	1423(3)	1602(4)	1707.2(7)	785.9(3)	3033(2)
ϱ_{calc}, g cm^{-3}	1.392(3)	1.436(4)	1.383	1.523	1.455
Z/Z'	4/1	4/1	4/1	2/1	8/2
Rwp (Rp), %	4.41 (5.99)	2.95 (3.93)	3.43 (2.55)	3.27 (2.17)	3.83 (4.97)
CCDC no.	2168832	2168833	2167407	2167408	2167409

Table 2. Crystallographic data for the newly determined DAN and FUR crystal structures obtained from single crystal X-ray analysis.

	DAN S_{EtOH}	DAN S_{NM}	DAN S_{DMC}	DAN S_{DXL}	DAN S_{THF} MH	DAN S_{DXN}	DAN S_{DMF}	DAN S_{DMSO}	DAN II	FUR I	FUR II	FUR III
Chemical formula	$C_{16}H_{16}N_4O_7$	$C_{15}H_{13}N_5O_7$	$C_{17}H_{16}N_4O_8$	$C_{16}H_{16}N_4O_7$	$C_{18}H_{18}N_4O_7$	$C_{18}H_{18}N_4O_7$	$C_{17}H_{17}N_5O_6$	$C_{16}H_{16}N_5O_6S$	$C_{14}H_{10}N_4O_5$	$C_{20}H_{16}N_8O_{10}$	$C_{10}H_8N_4O_5$	$C_{10}H_8N_4O_5$
Formula weight, g mol^{-1}	360.33	375.30	404.34	388.34	402.36	402.36	387.36	392.39	314.26	528.39	264.20	264.20
Temperature, K	150(2)	170(2)	170(2)	160(2)	170(2)	293(2)	293(2)	293(2)	293(2)	190(2)	190(2)	190(2)
Crystal system	Orthorhombic	Triclinic	Monoclinic	Monoclinic	Orthorhombic	Triclinic	Monoclinic	Monoclinic	Monoclinic	Triclinic	Monoclinic	Monoclinic
Space group	*Pbca*	*P*1	$P2_1/c$	$P2_1/c$	*Pbcn*	*P*-1	$P2_1/c$	*Cc*	$P2_1/c$	*P*-1	$P2_1/c$	$P2_1/c$
a, Å	13.9805(2)	8.3874(1)	11.9492(1)	4.8200(1)	29.212(9)	6.6913(3)	6.1686(4)	6.4223(5)	6.7682(2)	5.1078(2)	11.5684(3)	20.8403(15)
b, Å	10.2099(1)	8.8003(2)	11.7030(1)	20.3902(4)	12.787(9)	9.9570(5)	38.670(2)	38.739(4)	4.8498(2)	9.8921(3)	11.4705(3)	4.6778(3)
c, Å	22.8993(3)	11.5627(2)	12.8547(1)	17.6904(4)	10.401(3)	14.4356(6)	7.5270(5)	7.2089(7)	41.274(2)	22.7565(10)	8.3962(2)	11.4444(7)
α, °	90	94.670(1)	90	90	90	104.997(4)	90.00	90.00	90.00	80.534(1)	90.00	90.00
β, °	90	101.723(1	94.963(1)	97.654(2)	90	91.283(3)	91.875(6)	95.799(8)	91.082(3)	88.480(1)	106.0570(10)	93.479(3)
γ, °	90	101.361(1)	90	90	90	100.343(4)	90.00	90.00	90.00	76.452(3)	90.00	90.00
V, $Å^3$	3268.64(7)	812.70(3)	1790.88(3)	1723.14(6)	3885(3)	911.52(7)	1794.6(2)	1787.3(3)	1354.6(1)	1102.51(7)	1070.67(5)	1113.62(13)
ϱ_{calc}, g cm^{-3}	1.464	1.534	1.500	1.497	1.376	1.466	1.434	1.461	1.541	1.592	1.639	1.576
Z/ *Z'*	8/1	2/1	4/1	4/1	8/1	2/1	4/1	4/1	4/1	4/2	4/1	4/1
R1 (wR2), %	4.18 (10.68)	3.54 (9.97)	4.05 (11.24)	4.37 (11.50)	12.10 (36.30)	4.2 (12.2)	7.5 (21.8)	3.7 (10.0)	5.1 (18.9)	6.3 (19.3)	4.4 (10.4)	6.2 (13.1)
CCDC no.	2167411	2167413	2167412	2167410	2165775	2204148	2204149	2204150	2204147	910673	918796	929134

3.2 Properties of individual molecules

The formation of different crystal structures is associated with the ability of a molecule or molecules to pack in the solid state in different ways. In general, this can be related to the change of the conformation of the molecule and/or formation of different intermolecular interactions. Therefore, we firstly compare the likelihood of the studied molecules to adapt different conformations and the likelihood of the molecules to form different intermolecular interactions, including a quantitative evaluation of the electrostatic properties of molecular fragments in the most likely conformers.

Conformation and conformational energy

In previously published works reporting and discussing crystal structures of the studied compounds[31,32,53–58,60], different atom numbering approaches and conformer labels been used. To make the discussion easier, instead of using the atom numbering as in the original literature, here we introduce and use a common numbering scheme for all three analysed imidazolidine-2,4-dione derivatives to discuss the already published as well as the newly determined crystal structures. The atom numbering scheme used for all three compounds is given in Figure 1.

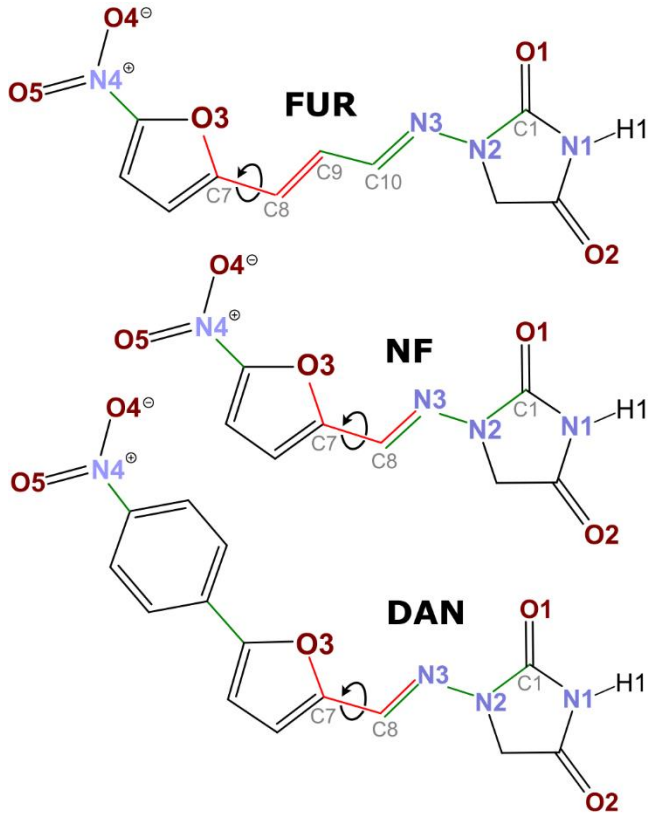

Figure 1. Molecular structures of FUR, NF and DAN showing the used unified atom numbering scheme, as well as highlighted in red is the torsion angle leading to the different conformers present in the crystal structures, and in green – potentially flexible torsion angles (or the middle bond of

such angles) adapting nearly identical value in all known crystal structures. Each atom type is numbered separately starting with 1, by firstly numbering atoms in the hydantoin ring, then atoms in the furan ring, followed by the atoms in the chain between the rings and for DAN also atoms in the benzene ring.

All three studied molecules contain torsion angles allowing the molecules to adopt different conformations. However, the molecular flexibility in all the molecules is limited because the molecular structure results in well-defined one or two minimums in the potential energy for all the flexible torsion angles. As a result, the nitro group in all molecules is always almost in plane with the adjacent furan or benzene ring, the benzene ring in DAN is almost in plane with the furan ring, and the two central double bonds in FUR adopt the most efficient *s-trans* conformation.

The two remaining torsion angles, which define the orientation of the furan ring and hydantoin ring with respect to the central double bond (or bonds in FUR), provide an almost planar conformation of the molecule. This corresponds to two different arrangements for each of the torsion angles. Therefore, 4 almost planar conformers are possible for all studied molecules. However, in all the experimental crystal structures the hydantoin ring always adopts a conformation with torsion angle C1-N2-N3-C8 (C1-N2-N3-C10 in FUR) close to 180°. Therefore, based on the known crystal structures, the only variable part is the torsion angle O3-C7-C8-N3 (O3-C7-C8-C9 in FUR) between the furan ring and the central double bond (or bonds in FUR) which is either ~0° (conformer A) or ~180° (conformer B), see conformers and their labels in Figure 2. Geometrically, the orientation of both rings and the double bond in conformer A results in O1, N3 and O3 atoms being positioned in the same direction resulting in formation of a pocket defined by mostly heteroatoms on this side of the molecule, whereas in conformer B O1 and O3 atoms are positioned in opposite directions and no such pocket is present.

Additionally, conformers in which the torsion angle C1-N2-N3-C8/C10 is ~0° and the torsion angle O3-C7-C8-C9/N3 is either ~0° or 180° are also shown to be energetically competitive and are designated as conformers C and D, respectively. Nevertheless, because these conformers are not present in any of the obtained crystal structures, they are not included in the further discussion throughout the article. Geometrically the relative arrangement of O1 and O3 atoms in these conformers are the same as that in conformers A and B, respectively, but O1 atom forms a weak intramolecular hydrogen bond with the neighbouring H atom (H atom at C8 for NF, DAN and C10 for FUR), which could prevent formation of as efficient intermolecular interactions as formed by conformers A and B, which could explain the absence of conformers C and D in the crystal structures.

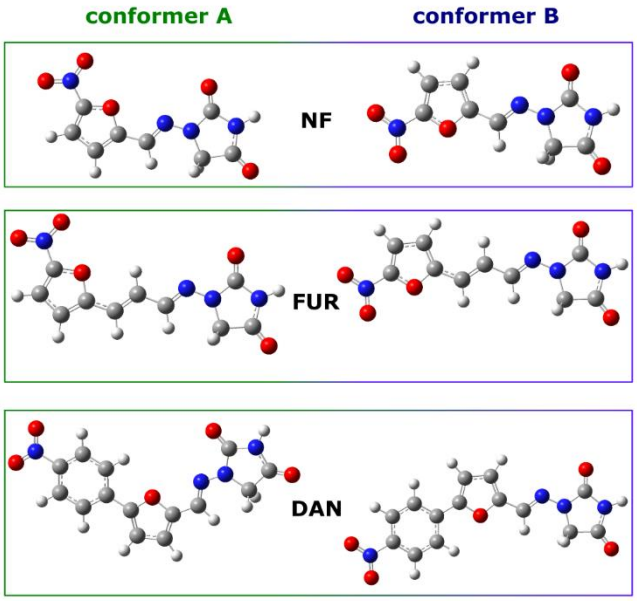

Figure 2. NF, FUR and DAN conformers A and B as found in the known crystal structures.

To compare the energy of NF, FUR and DAN conformers A and B, the Gibbs free energy was calculated, by performing geometry optimization and calculation of the thermal correction to Gibbs free energy in vacuum at the M06-2X/6-31++G(d,p) level and calculating the electronic energy for this geometry at the M06-2X/aug-cc-PVDZ level in vacuum or solvent modelled using a SMD continuum model. The obtained Gibbs free energy differences between both conformers are shown in Table 3.

Table 3. Calculated relative Gibbs free energy of NF, FUR and DAN conformers A and B in vacuum and selected solvent media.

Compound and conformation		Medium and $\Delta(\Delta G_{conf.})$, kJ·mol			
		Gas phase	water	DMSO	1,4-dioxane
NF	A	8.8	0	0	7.1
	B	0	1.7	1.4	0
FUR	A	0.0	0	0	0.7
	B	0	0.0	0.4	0
DAN	A	5.5	0.4	0.9	4.3
	B	0	0	0	0

For all three compounds these results indicate that in the gas phase and the relatively low polarity 1,4-dioxane medium conformer B is the lowest energy conformer. In fact, for DAN conformer B is the lowest energy conformer in all the used mediums, which agrees with the reported conclusion that the conformer B is the lowest energy conformation[53] (however, note the different conformer nomenclature in the literature). Nevertheless, in crystal structures conformer B is present only in

polymorphs DAN I and DAN III [53], whereas in all the other crystal structures conformer A is present (in total 19 out of 21 structures of single and multi-component phases).

For NF and FUR in highly polar medium, such as water or DMSO, the lowest energy conformer is conformer A. Despite this, conformer A is present in most of the known NF crystal structures (12 out of 13 known structures of neat and solvated NF) but only half of the known FUR structure (8 out of 14 known FUR structures, including two of the three FUR polymorphs).

On the basis of these results it can be concluded that for these compounds the relative energy of the conformers is not the dominant factor in determining the appearance frequency of the respective conformer in the crystal structures, as both conformers are energetically almost equally accessible for FUR, and, overall, the least stable of the two conformers dominated in crystal structures for NF and DAN. This is also supported by the NF conformer B being only present in a solvate with the polar DMSO, even though specifically in this solvent this conformer has the lowest relative stability, while in solvents where this conformer is calculated to be stable only structures with conformer A have been obtained.

An additional proof to the described conclusion is the Gibbs free energy of conformers C and D for DAN and NF which was calculated to be lower or similar to that of conformer B in the gas phase and low polarity solvent medium but are not present in any of the crystal structures. Therefore, apparently more important factor for conformer of 2,4-imidazolidine-2,4-dione derivatives to appear in the crystal structures are its ability to form efficient intermolecular interactions.

Overall, however, based on the analysis of torsion angles and the relative energy of the most likely conformers, all three studied molecules have similar access to conformational variability.

Charge distribution

As discussed above, the differences in prevalence of conformer A or B among the crystal structures of NF, FUR and DAN could be associated with the differences in the propensity to form different intermolecular interactions by these conformers. To evaluate this, electrostatic potential (ESP) surfaces of NF, FUR and DAN conformers A and B were calculated (see Figure 3). Conformers C and D were not analysed since these are not present in any of the known NF, FUR and DAN crystal structures.

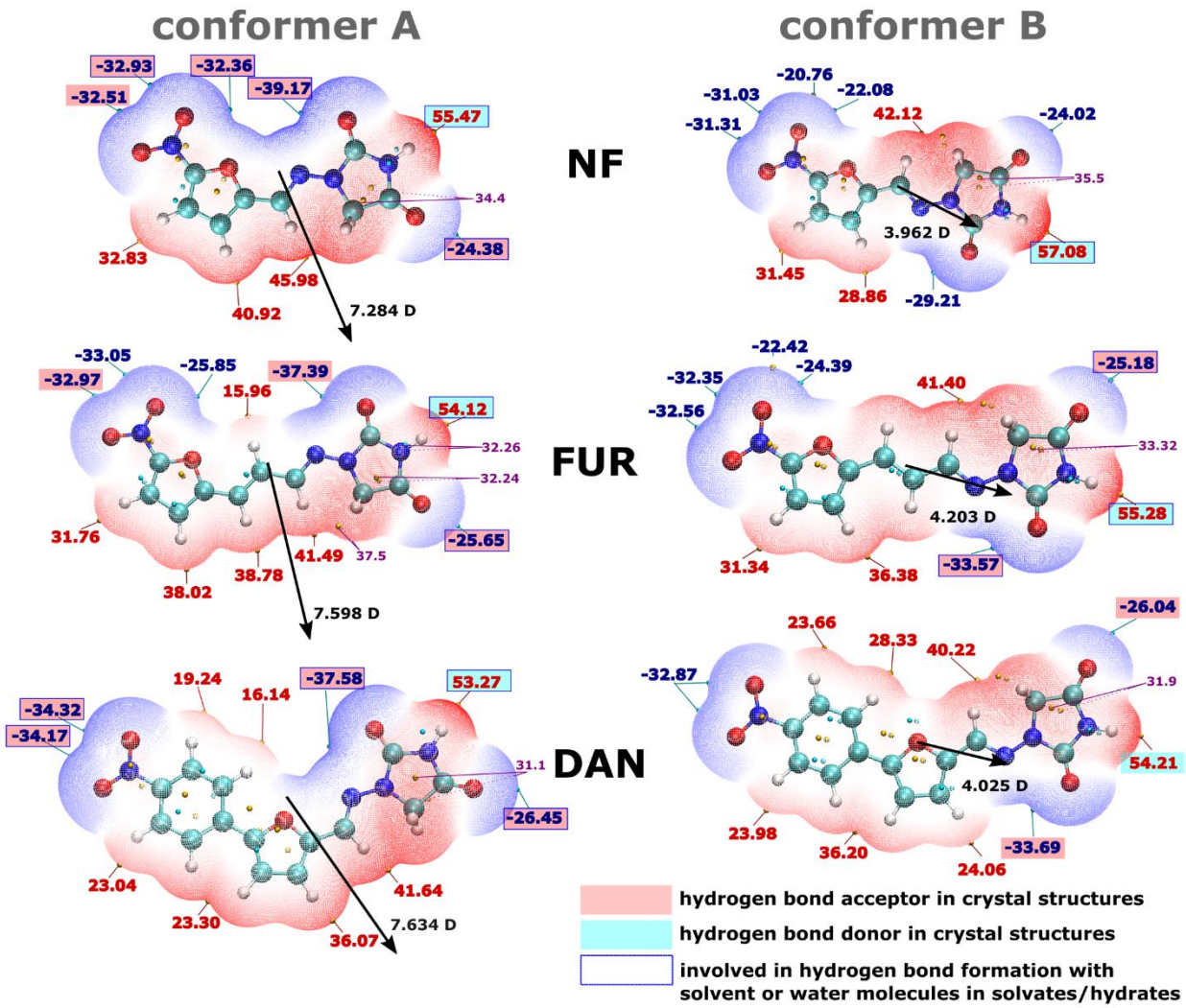

Figure 3. Electrostatic potential (ESP) surfaces of NF, FUR and DAN conformers A and B with ESP extrema values given in kcal·mol^{-1}. For each compound, numerical values of ESP extrema associated with the formation of a strong hydrogen bond are highlighted on the basis of their functionality. In black – calculated dipole moments in Debye and the vector of dipole moment.

Conformer A is more common in the crystal structures for all three compounds (12 out of 13 NF structures, 8 out of 14 FUR and 19 out of 21 DAN analysed crystal structures contain conformer A). The preponderance of the conformer A in the solid state over conformer B could be explained by the distribution of ESP extrema and positive and negative ESP surface regions: the negative region on heteroatoms (except for that on O2) throughout the molecule is concentrated on one side of the molecule (with a gap at C9 for FUR and C10, C11 for DAN) in conformer A, resulting in a distinct positive and negative side of the molecule. This observation is backed up by the calculated dipole moments, which for conformer A is almost two times larger than for conformer B. More specifically, by comparing conformers for each compound, the ESP extrema values on the heteroatoms are lower for conformer A. However, the calculated natural atomic charges (given in Table S2) contradict this observation: the values for the N1 and H1 atoms are unaffected by the

conformation, while the values for other heteroatoms do not show any clear conformation dependence.

It can therefore be speculated that packing of the molecules adopting more polar conformation A is more efficient or easier, and this could cause the preponderance of this conformer in the solid state.

3.3 Crystal structures of non-solvated phases

To get insight into the formation of crystal structures of the studied molecules, intermolecular interactions and their energy were compared for the experimental polymorphs of all the three studied compounds. This included crystallographic analysis of both known NF polymorphs, all 6 known DAN polymorphs, as well as 3 FUR polymorphs. The analysis of the experimental crystal structures is complemented by the analysis of the predicted structure landscapes formed by conformers A and B for all three of the compounds to get an insight in the appearance frequency of different hydrogen bonding patterns in larger number of structures.

Crystal structures of the experimental polymorphs

For all the already published and newly determined NF, FUR and DAN polymorphs we calculated the packing index, lattice energy as well as identified the strong hydrogen bonds and calculated the pairwise interaction energy for the molecule pairs linked by these interactions (see Table 4, the energy components (electrostatic, polarization, dispersion, and exchange-repulsion energies) of lattice energy and interaction energy are available in Table S4, Supporting Information). In all the structures of polymorphs only two different strong hydrogen bonds N1-H1···O1 and N1-H1···O2 are present, and characteristic examples for the hydrogen bond motifs observed are shown in Figure 4 a-d.

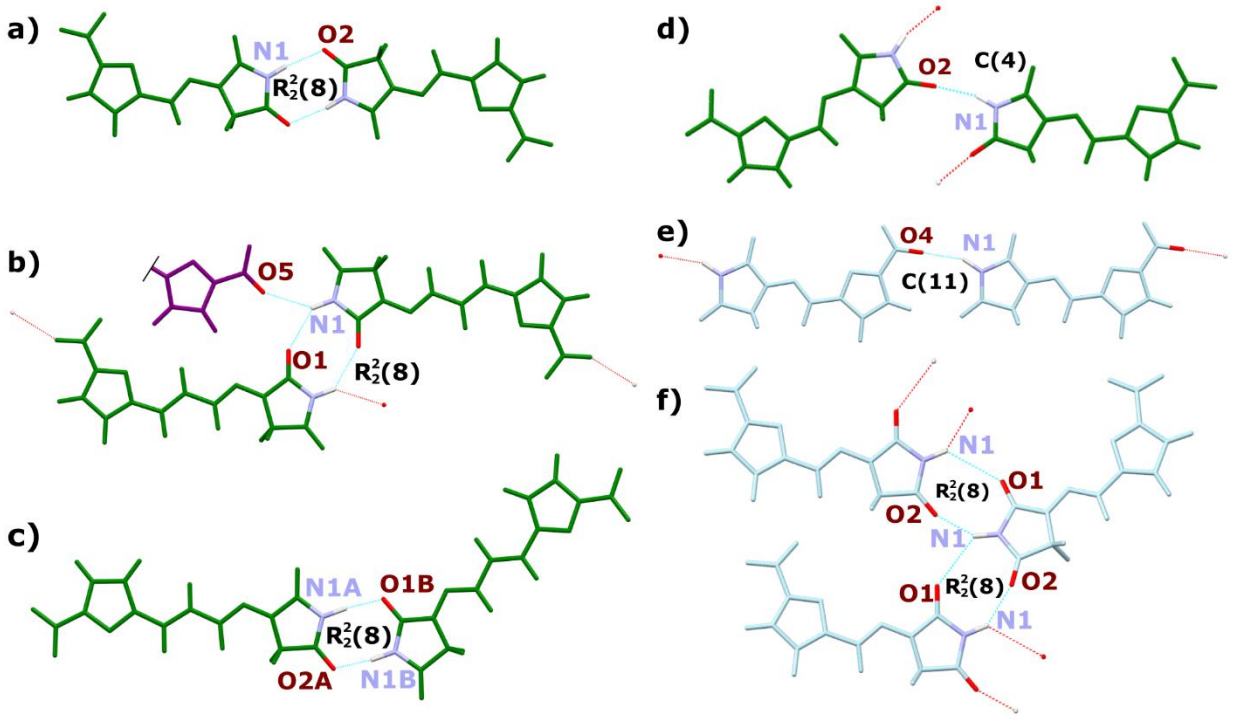

Figure 4. Examples of the hydrogen bond motifs formed by the strong hydrogen bonds N1-H1···O1 and N1-H1···O2 as found in structures of NF, FUR and DAN experimental polymorphs and the computationally generated structures in the CSP runs – a) $R^2_2(8)$ formed by N1-H1···O2 bond as in NF α; b) $R^2_2(8)$ formed by N1-H1···O1 bond and C(13) formed by N1-H1···O5 as in FUR II; c) $R^2_2(8)$ formed by both N1-H1···O1 and N1-H1···O2 bonds as in FUR I; d) C(4) formed by N1-H1···O2 bond as in NF β; e) C(11) formed by N1-H1···O4 bond as in the computationally generated structures of NF (similar motifs C(13) are formed by FUR and C(15) by DAN in their computationally generated structures); f) two $R^2_2(8)$ motifs formed by both N1-H1···O1 and N1-H1···O2 bonds as in the computationally generated structures of NF.

Table 4. Molecular conformation, packing index, lattice energy, the strong hydrogen bonds and the hydrogen bond motifs as well as the pairwise interaction energy for the hydrogen bonded molecule pairs in all the known NF, FUR and DAN polymorphs.

Phase	Conformer	Packing index, %	$E_{lattice}$, kJ·mol^{-1}	Interaction and associated graph set		E_{inter}, kJ·mol^{-1}
NF β	A	74.5	-176.3	N1-H1···O2	C(4)	-25.7
NF α	A	74.1	-176.9	N1-H1···O2	$R^2_2(8)$	-52.2
FUR I	B	71.9	-188.3	N1A-H1A···O1B N1B-H1B···O2A	$R^2_2(8)$	-56.7
FUR II	A	75.4	-186.5	N1-H1···O1	$R^2_2(8)$	-40.4
				N1-H1···O5	C(13)	-11.4
FUR III	A	72.4	-183.9	N1-H1···O2	$R^2_2(8)$	-54.8
DAN I	B	71.5	-196.9	N1-H1···O1	$R^2_2(8)$	-60.9
DAN II	A	69.9	-178.1	N1-H1···O2	$R^2_2(8)$	-54.0
DAN III	B	71.0	-191.6	N1-H1···O1	$R^2_2(8)$	-61.9
DAN IV	A	72.4	-179.6	N1-H1···N1	C(4)	-16.7
DAN V	A	72.3	-184.3	N1-H1···O2	C(4)	-33.6
DAN VI	A	71.2	-195.2	N1-H1···O2	$R^2_2(8)$	-54.5

Majority of NF, FUR and DAN polymorphs contain conformer A (8 out of 11 known structures). Both known polymorphs of NF contain conformer A and N1-H1···O2 as the strong hydrogen bond forming C(4) motif in the stable polymorph β whereas the $R^2_2(8)$ motif in the metastable α. All the other crystallographic parameters of both polymorphs shown in Table 4 are similar. The stable polymorph β has slightly better packing index (α form: 74,1%, β form: 74,5% kJ·mol^{-1}), but the metastable polymorph α has slightly lower lattice energy (α form: −176.9 kJ·mol^{-1}, β form: −176.3 kJ·mol^{-1}) and stronger N1-H1···O2 interaction energy (pairwise interaction energy corresponding to one N1-H1···O2 interaction is −26.1 kJ·mol^{-1} for α form and −25.7 kJ·mol^{-1} for β form).

For FUR and DAN, the most stable polymorphs contain conformer B (FUR I and DAN I) which in the previous section was determined as the lowest energy conformer in the gas phase and in low polarity (*e.g.,* 1,4-dioxane) medium. All three FUR polymorphs contain $R^2_2(8)$ hydrogen bond motif. FUR I is the only Z'=2 structure, the only structure simultaneously having both N1-H1···O1 and N1-H1···O2 hydrogen bonds and only FUR polymorph having conformer B. Furthermore, it has the strongest $R^2_2(8)$ N1-H1···O1/O2 interaction (pairwise interaction energy for the molecule pair −56.7 kJ·mol^{-1}) and the lowest lattice energy (−188.3 kJ·mol^{-1}) while having the lowest packing index (71.9%). The second of the two FUR polymorphs that form in cooling crystallization from pure solvent FUR II besides the N1-H1···O1 hydrogen bond forming motif $R^2_2(8)$ has an additional N1-H1···O5 hydrogen bond forming motif C(13) that apparently reduce the efficiency of the interaction between the molecules linked by N1-H1···O1 (which is only −40.4 kJ·mol^{-1}), while providing additional structural support and increasing the packing index (75.4%). FUR III, which can be obtained only under specific conditions (see Experimental section), has the least negative lattice energy (−183.9 kJ·mol^{-1}), which confirms its lower stability. Furthermore,

this is the only FUR polymorph that has a single N1-H1···O2 hydrogen bond which could explain the requirement for its specific preparation conditions.

DAN polymorphs DAN I, DAN II and DAN III can be directly obtained in crystallization[53], and all these polymorphs contain $R^2_2(8)$ hydrogen bond motif. Polymorphs DAN IV, DAN V and DAN VI are dehydrates of structurally similar DAN hydrates DAN H I, DAN H II and DAN H III[53], and two of these polymorphs contain N1-H1···O2 hydrogen bond forming either $R^2_2(8)$ or C(4) motif, whereas in DAN IV there is no conventional strong hydrogen bond.

Both DAN conformer B structures (DAN I and DAN III) contain hydrogen bonds N1-H1···O1 which are the strongest among the polymorphs (pairwise interaction energy per a molecule pair lower than −60 kJ·mol^{-1}). In contrast, conformer A structures contain hydrogen bond N1-H1···O2, except for DAN IV that contains a unique and rather inefficient unconventional intermolecular interaction N1-H1···N1. The most stable polymorph is DAN I also having the lowest lattice energy (−196.9 kJ·mol^{-1}).

Comparison of predicted crystal structure landscape

To gain insight into the tendency of the studied compounds to form different hydrogen bonding patterns, we used computationally generated Z′ = 1 crystal structure landscapes of NF, FUR and DAN conformers A and B. Such landscapes were accessible as a result of the previous studied for DAN[53] and FUR[54], whereas for NF crystal structure prediction was performed as a part of this study. From the computationally generated and optimized with CrystalOptimizer (for DAN and NF) or DMACRYS + *Gaussian16* (for FUR) structures 400 lowest energy structures were analysed for NF and DAN (covering energy range of 16 kJ·mol^{-1} for NF and 19 kJ·mol^{-1} for DAN with respect to the global energy minimum), and 354 structures for FUR (covering energy range of 18 kJ·mol^{-1}). Although the computational approach used for generating these landscapes is somewhat different for FUR (see Experimental Section), the overall approach is rather similar, including similar approaches used for the structure generation and geometry optimization steps, therefore we believe that all the structure landscapes as well as the results obtained from their analysis are comparable. The graphic representation of the computationally generated crystal structure landscapes of NF, FUR and DAN with different symbols used for each of the conformers as well as hydrogen bonding interaction type is shown in Figure 5. For detailed information on the appearance frequency of structures containing each conformer and each hydrogen bonding interaction see Table S3, Supporting Information.

We note that here we present and analyse computationally generated structure landscapes with intermolecular interaction energies calculated using the DMACRYS code. These were calculated to find a list of rather large number of low energy structures using similar computational approach for all compounds. Presenting the structure landscapes with the best possible accuracy of the relative energies was outside the scope of this study, and a more accurate structure landscape of DAN and FUR after DFT-D optimization is already available[54,53]. Therefore, the discussed relative energies of these structures are of secondary importance. Based on the DFT-D optimized structure

landscape of DAN[53] it can be concluded that overall the structures containing conformer A become energetically more competitive compared to structures containing B in agreement with most of the experimental structures containing conformer A (note that in[53] the opposite labelling of conformers is used).

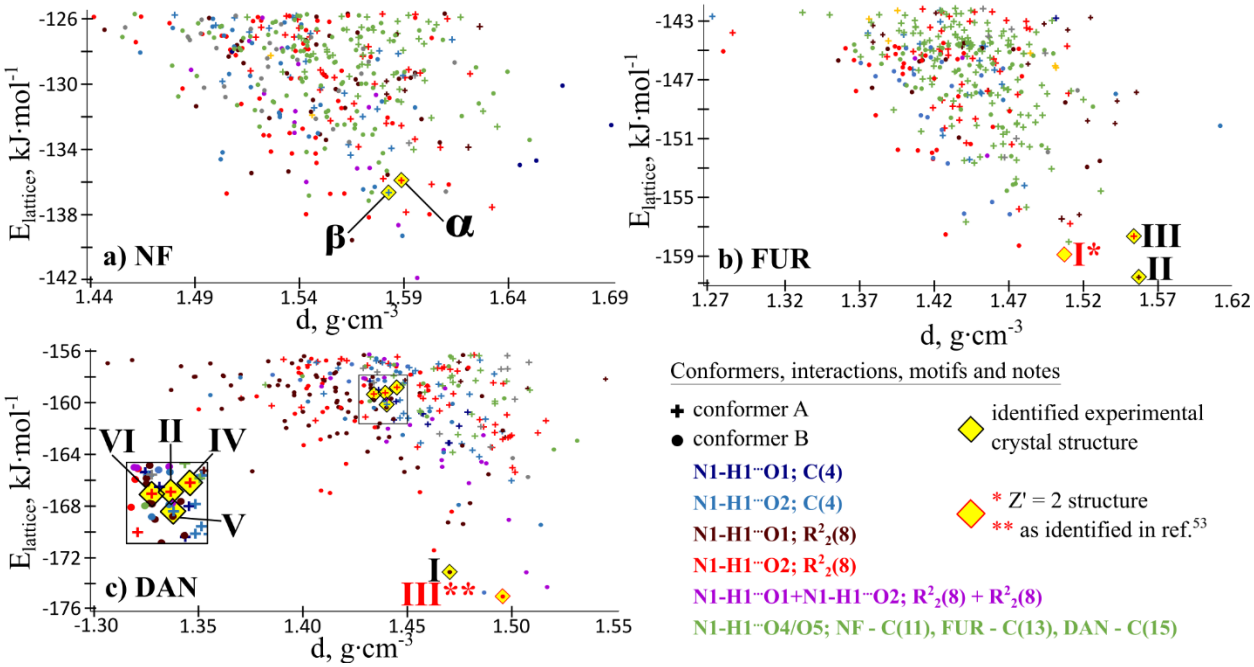

Figure 5. Computationally generated crystal structure landscapes of NF (a), FUR (b) and DAN (c) where each full symbol represents a stable lattice energy minimum. The conformation and hydrogen bond interactions present in each structure are coded by the used symbol and colour. The larger symbols correspond to structures of the experimental polymorphs which are labelled and linked with the computationally generated structure, where possible.

The crystal structure landscape of NF (Figure 5 a) calculated at the selected level shows that the experimental structures NF α and NF β are neither the lowest energy structures, nor the lowest energy structures formed by conformer A. In the crystal structure landscape of FUR (Figure 5 b) the lowest energy structure corresponds to the experimental polymorph FUR II. FUR I is not among the analysed computationally predicted structures, as it is a Z'= 2 structure, but was found in a Z'= 2 CSP search in the original study[54]. The computationally generated set of structures from the original study[54] did not contain the structure corresponding to FUR III. Even though the conformation in the original search only slightly differed from that in the FUR III, an additional CSP run using the conformation exactly as in FUR III generated FUR III structure with only slightly higher energy than that of the global energy minimum. Such a results should be highlighted as a warning that the CSP procedure can still sometimes miss a structure, which can occur without any clear reason and even using reasonably good starting geometry. The reasons standing behind this observation will be investigated in our future studies. In the crystal structure landscape of DAN (Figure 5 c) the lowest energy structure can be labelled as DAN III* – a structure highly similar to the experimental polymorph DAN III, but containing $R^2_2(8)$ motif formed by N1-H1···O2

interaction instead of N1-H1···O1 as in DAN III[53]. However, note that the more accurate DFT-D energy calculation approach notably alters the structure landscape, including the global energy minimum and the location of all the experimental polymorphs[53].

For NF and DAN, the global minimum structure as well as 71% of the analysed NF and 67% of DAN computationally generated lowest energy structures contain the lowest energy conformer B despite its low prevalence among the experimental NF structures. In contrast, the lowest energy structure as well as 63% of the analysed lowest energy computationally generated structures of FUR contain conformer A which was determined as the lowest energy conformer in polar media such as DMSO and water. Overall, the appearance frequency of the conformers in the structures correlates with their stability in the low polarity medium, where the relative stability of conformer B increases in a row FUR-DAN-NF. This is likely because typical organic crystals are a medium with rather low polarity, compared to that of polar solvents.[61] Nevertheless, structures with conformation A are appearing more frequently compared to the ratio which would be predicted by the energy difference in, e.g., 1,4-dioxane.

Analysis of hydrogen bond motif in the lowest energy computationally generated FUR and NF structures revealed that C(13)/C(11) chains formed by N1-H1···O4/O5 (see Figure 4 e) are the most frequently appearing interaction (60% of FUR conformer A, 41% of FUR conformer B, 39% of NF conformer B and 38% of NF conformer A structures). Despite the high appearance frequency in the predicted structures, no experimental structure contains such chains as the only hydrogen bond interaction. This could be linked to the lower efficiency of this interaction, and even if the overall structures could be energetically efficient, nucleation of such structures could be complicated by lower stability of clusters formed by small number of molecules. However, for DAN only 19% of conformer A structures contain N1-H1···O4/O5 C(15) chains while in conformer B structures the C(15) chain and N1-H1···O1 $R^2_2(8)$ motif are equally common (36% and 30% respectively). Note that the DFT-D calculated energies for DAN did not notably change energy of such structures compared to those containing hydrogen bonds N1-H1···O1/O2 and both interactions were frequently appearing among the low energy structures[53].

For DAN N1-H1···O2 interactions are favoured over N1-H1···O1 only for conformer A structures, whereas for NF and FUR N1-H1···O2 interactions are favoured over N1-H1···O1 in all the structures. Nevertheless, $R^2_2(8)$ is favoured over C(4) motif for all three compounds. Overall, this is consistent with the interactions present in the experimental structures, as most of the structures contain the $R^2_2(8)$ motif, NF and DAN conformer A structures contain the hydrogen bond N1-H1···O2 (except for DAN IV), whereas DAN conformer B structures contain the hydrogen bond N1-H1···O1. In FUR both N1-H1···O1 and N1-H1···O2 are observed in two of the crystal structures.

3.4 Crystal structures of hydrates

NF forms two hydrates and DAN forms four hydrates. In contrast, there is no information that FUR would form any simple hydrate, although based on the rather complex solid form landscape of FUR[59] formation of its hydrate under some specific condition cannot be excluded. The pairwise

interaction energies between molecules linked by hydrogen bonds in NF and DAN hydrates are collected in Table 5, while a graphic representation of the hydrogen bonds present in the hydrates is given in Figure 6. All six known hydrate phases contain conformer A, which can be related to this being the lowest energy conformer in water medium, as described above.

Table 5. Packing index and information of the strong hydrogen bonds and the pairwise interaction energy for the respective molecule pairs for the NF and DAN hydrates. Electrostatic, polarization, dispersion, and exchange-repulsion energy components for each molecule pair are given in Table S5.

Phase	Packing index, %	Interaction	$E_{inter,}$ kJ·mol^{-1}
NF H I	72.4	N1-H1···O_w	-44.4
		O_w-H_w···O2*	-27.3
		O_w-H_w···O2 **	-14.0
NF H II	71.8	N1-H1···O_w	-42.2
		O_w-H_w··· O1/N3/O3/O4 *	-29.2
DAN H I	73.2	N1-H1···O_w	-38.0
		O_w-H_w···O2	-29.7
		O_w-H_w···O_w *	-26.5
DAN H II	74.7	N1-H1···O_w	-41.1
		O_w-H_w···O2*	-29.3
		O_w-H_w···O2 **	-14.6
DAN H III	71.3	N1-H1···O2 ($R^2_2(8)$)	-55.4
		O_w-H_w···O1	-21.5
		O_w-H_w···O5	-13.0
DAN H IV	70.1	N1B-H1B···O_wB*	-40.3
		N1A-H1A···O_wA**	-36.9
		O_wA-H_wA···O1B**	-31.4
		O_wB-H_wB···O1A*	-25.5
		O_wB-H_wB···O4A *	-15.6

*, **, *** – asterisks are used to denote hydrogen bonds as presented in Figure 6.

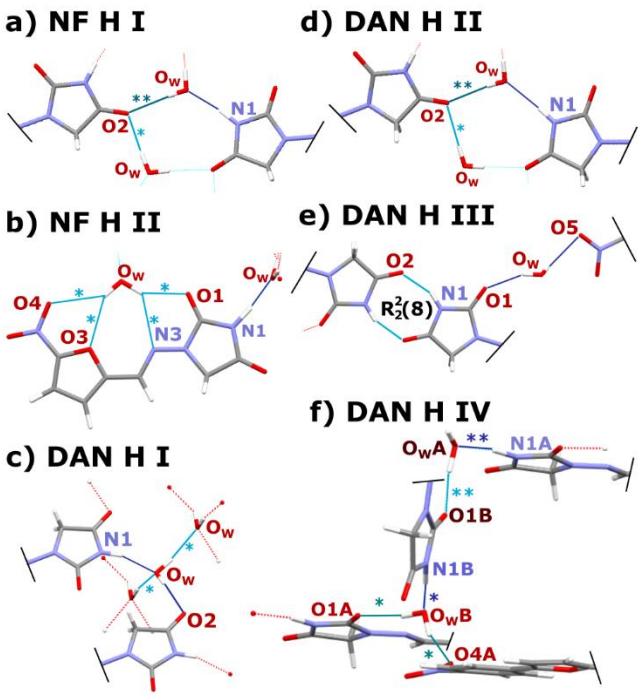

Figure 6. Graphic representation of hydrogen bonds in the NF and DAN hydrates presented in Table 3. Asterisks indicate the hydrogen bond designation as in Table 3. Figure with fully drawn molecules is given in Figure S2, Supporting Information.

DAN H III is the only hydrate in which the strong hydrogen bonds are formed between the host molecules, and it contains $R^2_2(8)$ motif formed by N1-H1···O2 interactions similarly as in polymorphs, whereas water is bonded by O_w-H_w···O1 and O_w-H_w···O5 hydrogen bonds (Figure 6 e).

In the other hydrates the host molecules forms strong hydrogen bonds only with the water molecules by forming strong hydrogen bond N1-H1···O_w (with pairwise energy for the molecule pair in the range from −36.9 kJ·mol^{-1} to −44.4 kJ·mol^{-1}), which in all the corresponding structures is accompanied by other hydrogen bonds – either two O_w-H_w···O2 hydrogens bonds (note the high similarity between NF H I and DAN H II as shown in Figure 6 a and d), hydrogen bonds O_w-H_w···O2 and O_w-H_w··· O_w (DAN H I, Figure 6 c), or by hydrogen bond O_w-H_w···O1 and other hydrogen bonds between water and other hydrogen bond acceptors (O_w-H_w··· N3/O3/O4 in NF H II, Figure 6 b, O_wB-H_wB···O4 in DAN H IV, Figure 6 f).

Hydrogen bonds present in the structure apparently affect the packing efficiency, as the structures containing N1-H1···O_w and O_w-H_w···O2 hydrogen bonds (NF H I, DAN H I, DAN H II) have higher packing index (72.4%, 73.2% and 74.7% respectively) than structures containing N1-H1···O_w and other hydrogens bonds (71.8% for NF H II and 70.1% for DAN IV) as well as structures not containing a N1-H1···O_w hydrogens bond (71.3% for DAN III).

3.5 Crystal structures of solvates

There are nine NF solvates with determined crystal structures, with crystal structures of 2-propanol (isopropyl alcohol, IPA) and benzyl alcohol (BnOH) solvates reported here for the first time. FUR has eleven reported solvated phases – seven solvates and four solvate-hydrates (heterosolvates containing organic solvent and water molecules). Three solvents (DMF, 1,4-dioxane and formic acid) form both a simple solvate and a solvate-hydrate. Crystal structures were determined for ten DAN solvates and one solvate-hydrate, with those of nine solvates and the solvate-hydrate reported here for the first time. All the solvated phases of NF and FUR are formed by solvents able to form strong hydrogen bonds, while DAN also forms solvates with other solvents. In Table 6, the packing index, conformation, strong hydrogen bonds and the interaction energy between the respective molecule pairs are given for all the analysed NF, FUR and DAN solvates and solvate-hydrates.

In crystal structures of the NF and FUR solvates with polar aprotic solvents (DMA, DMF and DMSO) there is only one strong hydrogen bond between the solvent and host molecules – N1-H1$\cdots$O$_{solv}$ (see Figure 7 a, e). FUR 1,4-dioxane solvate also contain N1-H1$\cdots$O$_{solv}$ bond but because of the symmetry, 1,4-dioxane in S$_{DXN}$ bonds to two FUR molecules by forming two identical hydrogen bonds. In NF solvates with alcohols (IPA, MeOH and BnOH) solvent molecules act as a linkers and NF molecules and solvent molecules form hydrogen bond chains $C^2_2(6)$ via two strong hydrogen bonds N1-H1$\cdots$O$_{solv}$ and O$_{solv}$-H$_{solv}\cdots$O2 (see Figure 7 b). This is true also for three of four FUR solvate-hydrates (FUR S$_{DMF}$MH, FUR S$_{DXN}$MH and FUR S$_{THF}$MH), which are structurally highly similar[59] and water molecule links FUR molecules forming N1-H1$\cdots$O$_w$-H$_w\cdots$O2 chains $C^2_2(6)$ (see Figure 7 f). In these solvate-hydrates FUR molecule is not directly bonded to the organic solvent molecule but acts as a linker providing additional O$_w$-H$_w\cdots$O$_{solv}$ bond.

Notably different from NF solvates and other FUR solvates are FUR formic acid solvated phases. In S$_{HCOOH}$ FUR molecules do not form any hydrogen bonds with the solvent molecules. Instead, FUR molecules form C(4) chain formed by N1-H1$\cdots$O2 hydrogen bonds as observed in polymorphs NF β and DAN V, and formic acid molecules form a parallel C(4) chain form hydrogen bonds O$_{HCOOH}$–H$_{HCOOH}\cdots$O$_{HCOOH}$=C$_{HCOOH}$. Unlike other solvate-hydrates of FUR, in S$_{HCOOH}$MH, there is a direct strong hydrogen bond between FUR and the organic solvent N1-H1$\cdots$O$_{HCOOH}$=C, and the water molecule bonds to two host units (employing hydrogen bonds O$_w$-H$_w\cdots$N3 and O$_w$-H$_w\cdots$O1) and formic acid molecule (O$_{HCOOH}$–H$_{HCOOH}\cdots$O$_w$), see Figure 7 f.

In contrast to NF and almost all FUR solvates, only part of the DAN solvates (DAN S$_{EtOH,}$ DAN S$_{DXL,}$ DAN S$_{DMF,}$ and DAN S$_{DMSO}$) contain N1-H1$\cdots$O$_{solv}$ hydrogen bond. Moreover, arrangement of solvent molecules with respect to the host molecules differs from that in NF and FUR solvates even in part of these solvates – although the solvent molecule in DAN S$_{EtOH,}$ DAN S$_{DXL}$ is positioned directly toward the hydantoin ring, due to the curvature of the DAN molecule, another DAN molecule is wrapped around the solvent molecule in a perpendicular direction to the N1-H1$\cdots$O$_{solv}$ hydrogen bond. Such positioning leads to differences in the spatial arrangement of the second hydrogen bond formed by the solvents as in DAN S$_{EtOH}$ (see Figure 7 c). Similar spatial

arrangement of hydrogen bonding as in DAN S_{EtOH} is also present in DAN S_{THF} MH where the water molecule connects two DAN molecules by hydrogen bonds O_w-H_w···O1 and O_w-H_w···N3 and acts as a linker for the solvent via the hydrogen bond O_w-H_w···O_{solv}, similar as in FUR solvate-hydrates, see Figure 7 g.

Majority of DAN solvates, however, contain hydrogen bonds N1-H1···O1/O2 linking DAN molecules as in polymorphs – five of the solvates contain $R^2_2(8)$ hydrogen bond motif (DAN S_{DXN} and DAN S_{DMC} contain N1-H1···O1 bond as in DAN I and DAN III, whereas DAN S_{NM}, DAN S_{MeOH} and DAN S_{HCOOH} contain N1-H1···O2 bond as in DAN II and DAN VI) and the solvent molecule is located in the cavity created by the curved DAN molecules and linked to the DAN by weak hydrogen bonds. DAN S_{ACN}, however, contain C(4) motif formed by hydrogen bonds N1-H1···O1 as in NF β (DAN V contains similar C(4) supramolecular chain formed by N1-H1···O2 interaction). Therefore, a strong hydrogen bond between DAN and solvent molecules is not essential in any of these solvates (see Figure 7 h). We note that the appearance frequency of the ring motif $R^2_2(8)$ and chain motif C(4) in solvate structures agree with the occurrence of these motifs in experimental and also computationally generated structures of DAN polymorphs.

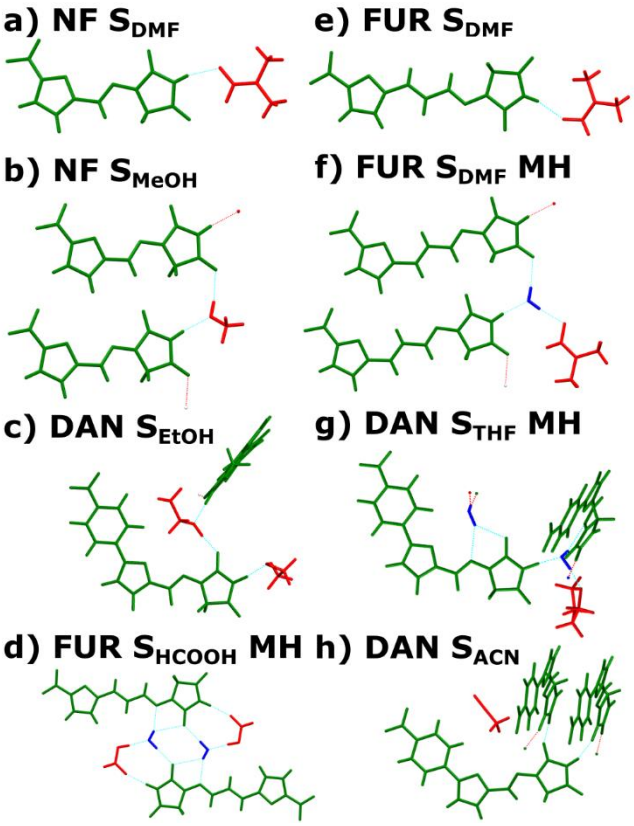

Figure 7. Graphic representation of characteristic strong hydrogen bonds and other host – guest interactions in solvates and solvate-hydrates of NF (a and b), DAN (c, g and h) and FUR (d-f).

Table 6. Packing index, molecule conformation and information of the strong hydrogen bonds and the pairwise interaction energy for the respective molecule pairs for all known NF, FUR and DAN solvated phase crystal structures. Electrostatic, polarization, dispersion, and exchange-repulsion energy components for each molecule pair are given in Table S6-S8, Supporting Information.

Phase	Packing index, %	Conformer	Interaction	$E_{inter,}$ kJ·mol^{-1}
NF S_{DMA} I	70.1	A	N1-H1···O_{solv}	-56.8
NF S_{DMA} II	73.5	A	N1-H1···O_{solv}	-53.3
NF S_{DMA} III	72.9	A	N1-H1···O_{solv}	-52.7
NF S_{DMF}	69.8	A	N1-H1···O_{solv}	-52.3
NF S_{DMSO}	71.7	A	N1-H1···O_{solv}	-52.0
NF $S_{0.5\ DMSO}$	– *	B	N1-H1···O_{solv}	– *
NF S_{IPA}	66.9	A	N1-H1···O_{solv} O_{solv}-H_{solv}···O2	-47.5 -25.0
NF S_{MeOH}	75.2	A	N1-H1···O_{solv} O_{solv}-H_{solv}···O2	-45.2 -26.3
NF S_{BnOH}	69.0	A	N1-H1···O_{solv} O_{solv}-H_{solv}···O2	-35.7 -25.6
FUR S_{DMSO} I	69.9	A	N1-H1···O_{solv}	-45.0
FUR S_{DMSO} II	70.2	A	N1A-H1A···O_{solv}A N1B-H1B···O_{solv}B N1C-H1C···O_{solv}C	-39.6 -45.1 -46.0
FUR S_{DMSO} III	70.2	B	N1-H1···O_{solv}	-46.5
FUR S_{DMA}	68.7	B	N1-H1···O_{solv}	-52.9
FUR S_{DMF}	70.0	B	N1A-H1A···O_{solv}A N1B-H1B···O_{solv}B N1C-H1C···O_{solv}C N1D-H1D···O_{solv}D	-49.9 -49.9 -42.5 -43.0
FUR S_{DMF} MH	70.2	A	N1-H1···O_w O_w-H_w···O2 O_w-H_w···O_{solv}	-43.8 -27.6 -33.5
FUR S_{DXN}	70.8	B	N1-H1···O_{solv}	-40.3
FUR S_{DXN} MH	71.0	A	N1-H1···O_w O_w-H_w···O2 O_{solv}-H_{solv}··· O_w	-44.4 -25.7 -27.4
FUR S_{THF} MH	69.4	A	N1-H1···O_w O_w-H_w···O2 O_w-H_w···O_{solv}	-45.0 -26.7 -28.4
FUR S_{HCOOH}	72.8	A	N1-H1···O2 C(4) O_{solv}-$H_{solv.}$·· O_{solv}	-25.4 -46.4
FUR S_{HCOOH} MH	70.6	B	N1-H1···O_{solv} O_w-H_w···O1 O_w-H_w···N3 O_{solv}-H_{solv}··· O_w	-31.2 -24.2 -37.0 -49.5
DAN S_{DXL}	73.5	A	N1-H1···O_{solv}	-39.3

DAN S_{DMF}	72.5	A	N1-H1···O_{solv}	-46.6
DAN S_{DMSO}	71.7	A	N1-H1···O_{solv}	-45.5
DAN S_{EtOH}	73.5	A	N1-H1···O_{solv} O_{solv}-H_{solv}···O1	-40.5 -34.1
DAN S_{ACN}	69.7	A	N1-H1···O1 C(4)	-29.3
DAN S_{DXN}	73.4	A	N1-H1···O1 $R^2_2(8)$	-62.6
DAN S_{DMC}	73.6	A	N1-H1···O1 $R^2_2(8)$	-63.3
DAN S_{NM}	73.6	A	N1-H1···O2 $R^2_2(8)$	-85.3
DAN S_{MeOH}	71.8	A	N1-H1···O2 $R^2_2(8)$ O_{solv}-H_{solv}···O1	-53.8 -26.2
DAN S_{HCOOH}	72.9	A	N1-H1···O2 $R^2_2(8)$ O_{solv}-H_{solv}···O5	-56.0 -10.2
DAN S_{THF} MH	70.6	A	N1-H1···O_w O_w-H_w···O1/N3 O_w-H_w···O_{solv}	-41.9 -29.3 -30.8

* - Calculations are not possible due to the disorder present in the structure

For solvate structures, additional insight into crystal structure formation was achieved by analysing molecule packing and energy-framework diagrams constructed using pairwise interaction energies calculated with CrystalExplorer.

From the energy-framework complemented packing diagrams (diagrams for NF S_{IPA}, NF S_{BnOH} and NF S_{DMF} are shown in Figure 8, and those for all NF solvates in Figure S3 and S4, Supporting Information) it can be seen that a characteristic feature of NF solvate crystal structures are molecular layers. On the horizontal direction, as represented in Figure 8 a-c, NF and solvent molecules form strong hydrogen bonds N1-H1···O_{solv} (dominated by electrostatic energy) whereas on the vertical direction the molecules are stacked, forming layered structure from NF molecule planes in alternating directions as in NF $S_{IPA,}$ NF S_{DMA} I, NF S_{DMA} III, NF $S_{DMF,}$ Figure 8 a,c or in a regular *zig zag* pattern as in NF $S_{MeOH,}$ NF $S_{BnOH,}$ NF $S_{DMSO,}$ Figure 8 b. This stacking is dominated by the dispersion energy. In nearly all solvate structures the packing motif is identical also in the perpendicular direction to the plane of the picture, and solvent molecules reside in channels or 2D layers of the resulting layered structure. Only NF S_{DMA} II in the perpendicular direction is constructed by two alternating orientations of the layered arrangement, and solvent molecules reside within pockets (similar packing is also present for FUR S_{DMF}, Figure 9 b).

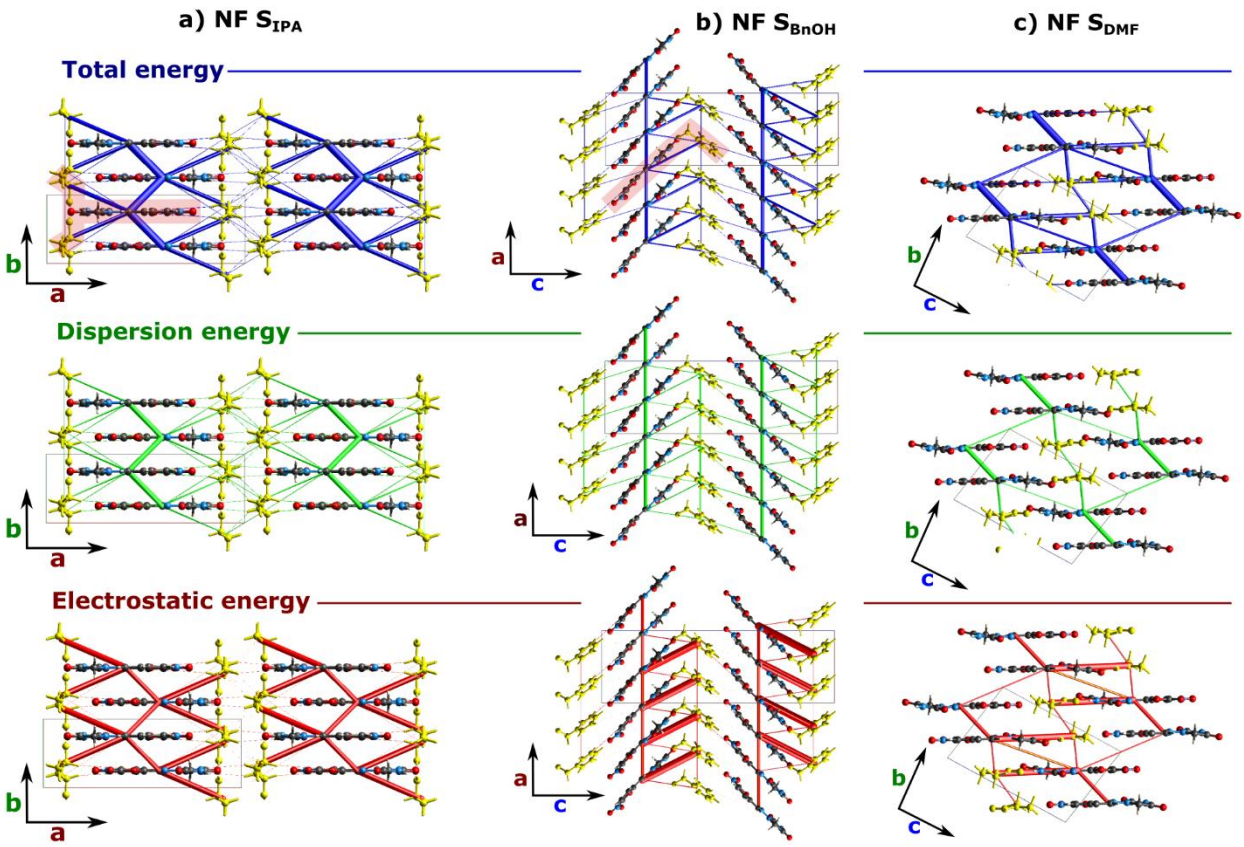

Figure 8. Energy-framework complemented packing diagrams showing E_{ele}, E_{dis} and E_{tot} for a) NF S_{IPA}, b) NF S_{BnOH}, c) NF $_{DMF.}$ All diagrams use the same cylinder scale of 40 for energies.

The energy-framework complemented packing diagrams of FUR solvated phases (for FUR S_{DMF}, FUR S_{DMF}MH shown in Figure 9, and other FUR solvates in Figure S5 and S6, Supporting Information) show similarities to packing in NF solvates– planar molecule arrangement in the FUR solvates and solvate-hydrates results in stacking of FUR molecules dominated by the dispersion energy to be a notable feature of the structures. Within the layers the molecules are bonded by the strong hydrogen bonds N1-H1···O_{solv} for which the electrostatic energy is the dominant component. Furthermore, packing in FUR S_{DMSO} I is almost identical to that in NF S_{IPA} (given in Figure 8 a), whereas FUR S_{DMSO} III resemble NF S_{DMA} and NF S_{DMF} solvates (Figure 8 c). The differences in the packing between these FUR and NF solvates are caused by the steric differences of the solvent molecules. Alternating criss-crossed packing molecule layers as in NF S_{DMA} II are found in FUR S_{DXN} and FUR S_{DMF} (Figure 9 a). Introduction of water molecules (as 1,4-dioxane and DMF are solvents that form both solvates and solvate-hydrates), however, allows the formation of planes as in FUR S_{DXN}MH, FUR S_{DMF}MH, and FUR S_{THF} MH (see Figure 9 b). Interestingly, FUR adopts different conformations in solvates and solvate-hydrates formed by the same solvent.

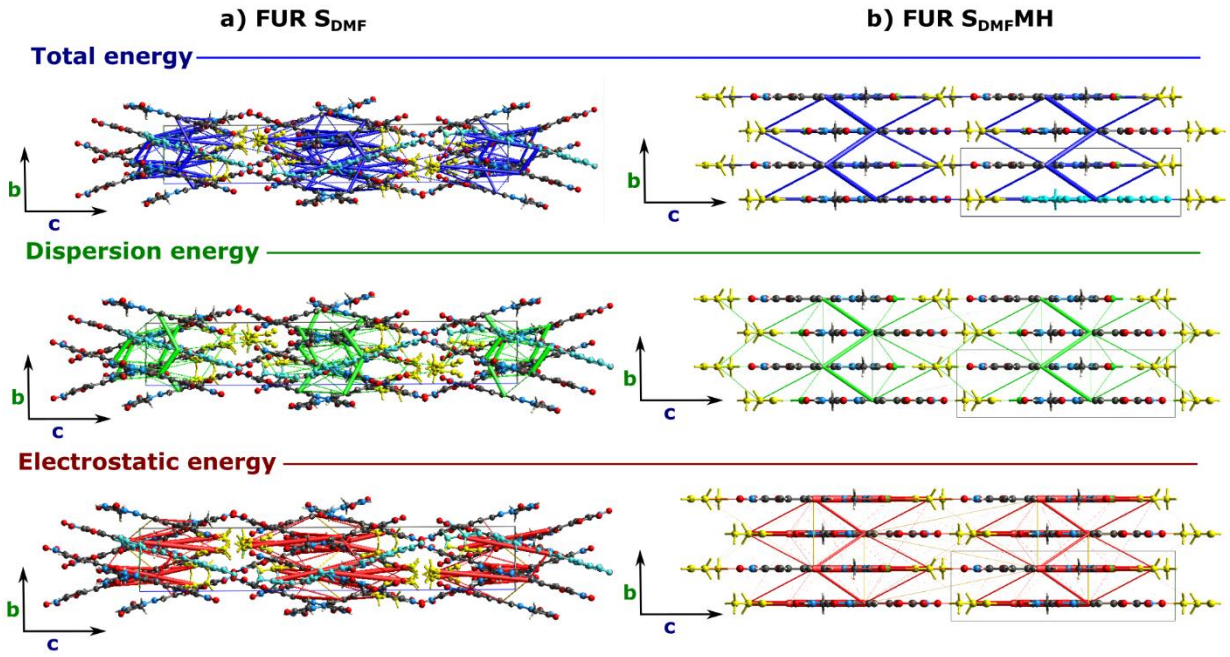

Figure 9. Energy-framework complemented packing diagrams showing E_{ele}, E_{dis} and E_{tot} for a) FUR S_{DMF}, b) FUR S_{DMF}MH. All diagrams use the same cylinder scale of 40 for energies.

Unlike FUR and NF solvates, the energy-framework complemented packing diagrams of DAN (DAN S_{DMSO} and DAN S_{ACN} shown in Figure 10, all DAN solvates shown in Figures S7 – S9, Supporting Information) show that the packing of the N1-H1···O_{solv} hydrogen bond containing DAN solvates is based on the electrostatic energy of N1-H1···O_{solv} hydrogen bonds and supplemented by dispersion interactions between the hydrogen-bonded molecular layers (Figure 10 a). The contribution of the dispersion energy between the hydrogen bonded molecular layers and the electrostatic energy of the N1-H1···O_{solv} hydrogen bonds to the total energy is highly similar.

Although layers are a characteristic feature of DAN solvate structures (as it was for NF and FUR solvates), due to the steric differences of the DAN molecules as described above, the layers are notably more complex and more structure specific than in NF and FUR solvates (see Figure 10 b), thus description of the formation of these structures from the perspective of formation of layers is ambiguous and therefore not attempted.

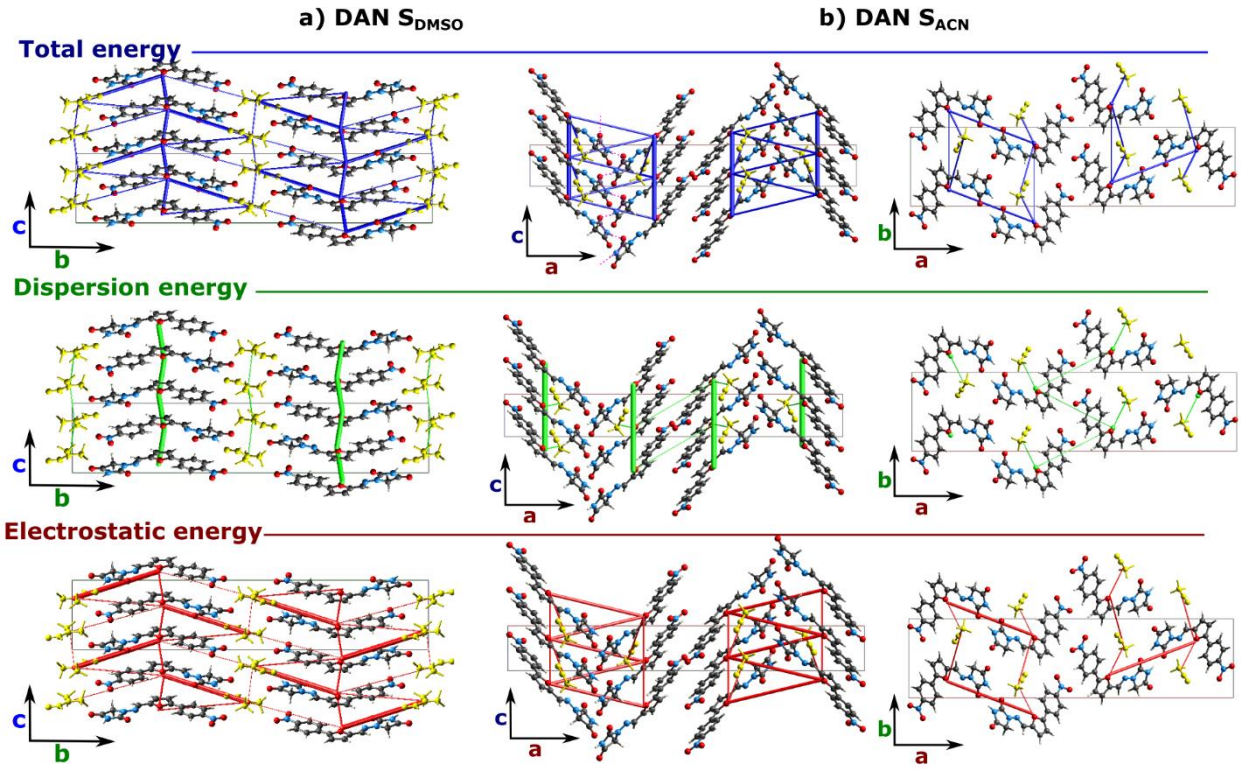

Figure 10. Energy-framework complemented packing diagrams showing E_{ele}, E_{dis} and E_{tot} for a) DAN S_{DMSO} and b) DAN S_{ACN}. All diagrams use the same cylinder scale of 40 for energies.

3.6 Discussion

Overall, based on the solid forms obtainable in the conventional crystallization experiments using cooling and evaporation crystallization from numerous commonly used solvents, as well as phase stability experiments, we see that NF has the lowest propensity to form different solid forms – despite the performed extensive crystallizations [62–64] (including mechanochemical synthesis[26] and crystallization from the melt of co-crystals[65]) only two polymorphs were observed. Furthermore, the extensive crystallizations of NF from water containing solvents[66–70] produced only two hydrates, whereas solvate formation was observed only with very strong hydrogen bond acceptors (DMF, DMA and DMSO), and part of the alcohols that are hydrogen bond donors and acceptors[64].

In contrast, three polymorphs were obtained for FUR, with preliminary results suggesting the existence of other FUR polymorphs not yet fully explored. However, no hydrate for FUR was obtained, meaning there is no stable hydrate for this compound. Nevertheless, FUR showed higher propensity to form solvates, as, if compared to NF, FUR also forms solvates with weaker hydrogen bond acceptor 1,4-dioxane, formic acid as well as several solvate-hydrates[59]. Conversely, DAN had the highest propensity to form different solid forms, as six polymorphs, four hydrates, ten solvates formed by solvents with notably different properties as well as a solvate-hydrate was

characterized structurally, and formation of several other solvates, solvate-hydrates and hydrates was observed, with these phases not fully or just structurally characterized[53].

Generally, the number of polymorphs which could be obtained for a compound is in no way straightforward to be predicted or rationalized, as this is determined not only by the stability of the theoretical structures, but also by factors such as effect of potential structure disorder on the thermodynamic stability, nucleation and growth rate and mechanisms of these phases and relative stability with respect to the multicomponent phases under the conditions of formation[71]. Therefore, even though the accuracy of the crystal structure prediction methods is increasing[72] and approaches for obtaining free energy landscapes of structures are being searched, *e.g.,* incorporation of the effects from the structure disorder by correcting the polymorph energy landscapes[73], by approaching ability to answer whether additional polymorphs can be expected to be obtained for well-studied polymorphic compounds[74], prediction of nucleation and growth rates and limitations associated with these factors in obtaining polymorphs are still unreliable or even impossible[75,76].

Therefore, we do not intend to rationalize the differences in the number of polymorphs formed by each compound. Clearly, all three compounds can form highly similar intermolecular interactions, as shown by the ESP analysis, and the obtained experimental and computationally generated structures demonstrate that this is mostly confirmed by the crystal structures. Similarly, all compounds have and employ similar conformational variability in the crystal structures. Nevertheless, we noted two differences among the compounds that correlate with the number of polymorphs obtained. First, overall, both NF polymorphs showed a very high packing efficiency, which could correlate with the low propensity to crystallize in other crystal structures. Second, NF is the smallest of the molecules allowing the least potential modes for packing, whereas DAN is the largest, and has a curved molecular shape, which potentially allows more packing possibilities that could result in more energetically competitive differently packed structures. Additionally, different DAN polymorphs obtained in the desolvation of solvates[53] could be formed because of larger energy barrier associated with the structural reorganization to one of the stable polymorphs by these relatively larger molecules. Nevertheless, the computationally generated structure landscapes show equal number of hypothetical structures accessible for all the studied compounds, and it is unlikely that better energy model would significantly affect this.

Altogether, on the basis of the structural features present in most of the hydrates, there are no visible factors that could result in clear differences in tendency to form hydrates by the studied molecules. The only clearly exclusive interaction type is present in the stable NF hydrate H II, which could not be formed by FUR because of the notably larger separation of hydantoin and furan rings. In addition, the ESP properties of the molecules did not reveal factors preventing formation of a stable FUR hydrate. Similarly, the comparison of several potential host-water dimers showed no difference in the interaction energy between such dimers formed by NF easily forming a stable hydrate and FUR (see Table S9, Supporting information). Nevertheless, crystallization in the presence of water (*e.g.* solvent/water mixtures) and even suspending in water never resulted in formation of a FUR hydrate. Meanwhile, under identical conditions usually NF H II or, depending on the conditions, DAN H I, H II and H III are easily formed, while NF H I nucleates only under specific conditions. Therefore, the differences in hydrate formation could be associated with the

packing efficiency differences for structures with and without water, and it is likely that the structures in which FUR is packed with water are not energetically competitive to alternative FUR polymorphs or other solvated phases. Alternatively, the nucleation rate of the most stable FUR hydrate structures could be uncompetitive under the conditions where this phase would be thermodynamically feasible.

The cause of the different propensities in solvate formation among the studied molecules likely is different possibilities and efficiency of packing together with solvent. First, we note that the packing efficiency of NF solvates is lower or even notably lower than that of NF polymorphs (note that structure of S_{MeOH} is determined at 110 K). Therefore, the highly efficient packing of neat NF and the inability to form as efficiently packed structures together with solvent would explain the rather low propensity to form solvates, with solvates being obtained only in case of highly efficient intermolecular interactions as formed by strong hydrogen bond donors and alcohols could compensate for the mostly less efficient packing.

Also, FUR is not particularly keen to form solvates with different solvent molecules as, if compared to NF, additional solvates are obtained only with still very good hydrogen bond acceptor 1,4-dioxane and efficient hydrogen bonding forming formic acid. This could be because in FUR solvates, solvent molecules are also located in-between the planar FUR molecule layers, as in the case of NF solvates. Such arrangement still does not provide more efficient packing compared to the solvates, although the difference in the packing efficiency compared to FUR polymorphs is minor, which overall allows formation of solvates with additional solvent molecules, which is additionally supported by preliminary results suggesting existence of solvates with few other solvents.

The most notable difference in FUR solvate formation compared to NF is the propensity to form solvate-hydrates. The formation of such structures can be rationalized in terms of highly efficient hydrogen bonding in these structures, making these structures energetically feasible. As based on the performed analysis there is no clear reason why such structures could not be formed also by NF, the most likely reason is the very high stability of NF hydrate H II, which is obtained in crystallization experiments from solvent mixtures containing water. This is supported by its exclusive crystallization from water containing solvent mixtures[68,70] and also very high thermal stability (see Figure S11, Supporting information).

As described above, DAN has the highest propensity to form solvates, which is explained by the grater variability in the molecular packing resulting from the curved shape of this molecule. Therefore, the solvent can be arranged in the same way as in NF and FUR solvates or also by positioning the solvent in the cavities created by the curved DAN molecules, which allow formation of solvates with solvent linked by just weak intermolecular interactions. This explains both the formation of the largest number of solvates as well as the solvate formation with solvents having notably different properties. Additionally, the larger packing variability probably also explain the ability of DAN to form several different hydrate structures. Moreover, the formation of solvates of DAN is also facilitated by the packing efficiency, as in most of the solvates it is slightly improved if compared to that in the most stable polymorphs.

Furthermore, DAN rather easily forms solvate-hydrates, as, even though only S_{THF} MH is structurally characterized, solvate-hydrates containing acetone and 2-butanone (methyl ethyl ketone) have also been obtained[53]. This could be explained by the fact that small amounts of water in the solvent of crystallization does not exclusively result in formation of one of the hydrates, as observed for NF, as well as by the lower stability of DAN hydrates obtained in crystallization experiments in presence of water[53] if compared to NF H II (see Figure S11, Supporting information).

4 CONCLUSIONS

All three analysed marketed drugs, nitrofurantoin, furazidin and dantrolene, share similar conformational variability in the crystal structures and can form highly similar intermolecular interactions, as demonstrated by the ESP analysis and the experimentally obtained and computationally generated structures of polymorphs. The molecule size, molecular shape and packing efficiency in neat polymorphs correlate with the propensity to crystallize in other crystal forms, particularly, solvates, which increases in a row NF-FUR-DAN. The highly efficient packing of neat polymorphs and inability to form as efficiently packed structures with solvent molecules explain the rather low propensity of NF to form solvates. In contrast, the ability of DAN to pack in several different ways resulted by the curved shape of this molecule could explain the notably higher diversity and larger number of DAN solvates. The easy formation of solvate-hydrates by FUR and DAN can be explained by highly efficient hydrogen bonding in such phases, whereas the very stable NF H II prevents the obtaining any NF solvate-hydrate. However, clearly detectable factors resulting differences in tendency to form hydrates by the studied compounds and factors preventing formation of a stable FUR hydrate could not be identified by the performed analysis.

Hopefully, the results described herein will pave the way toward systematic investigations of crystalline forms of pharmacologically relevant compounds prepared in academic settings, in view of their potential use and further development for drug manufacturing.

ASSOCIATED CONTENT

The Supporting Information (PDF) is available free of charge on the ACS Publications website at DOI: XXXX and contains description of mechanochemical preparation of DAN, additional and more detailed results from analysis of crystal structures of polymorphs, hydrates and solvates and computationally predicted crystal structure landscapes as well as thermal characterization of hydrates.

Accession Codes

CCDC 910673, 918796, 929134, 2165775, 2167407 – 2167413, 2168832, 2168833, 2204147 – 2204150 contain the supplementary crystallographic data for this paper. These data can be obtained free of charge via www.ccdc.cam.ac.uk/data_request/cif, or by emailing

data_request@ccdc.cam.ac.uk, or by contacting The Cambridge Crystallographic Data Centre, 12 Union Road, Cambridge CB2 1EZ, UK; fax: +44 1223 336033.

AUTHOR INFORMATION

Corresponding Authors

* Agris Bērziņš – *Faculty of Chemistry, University of Latvia, Riga, LV-1004, Latvia;* E-mail: agris.berzins@lu.lv; Telephone: +(371)-67033903.
* Aija Trimdale-Deksne – *Faculty of Chemistry, University of Latvia, Riga, LV-1004, Latvia;* E-mail: aija.trimdale@lu.lv; Telephone: +(371)-67033907.

Funding Sources

This work has been supported by the Latvian Council of Science, project "Crystal engineering of pharmaceutical multicomponent phases for more efficient crystalline phase design", project No. lzp-2018/1-0312.

Notes

The authors declare no competing financial interest.

ORCID, emails

Aija Trimdale-Deksne : 0000-0003-4285-0524 ; aija.trimdale@lu.lv

Artis Kons : 0000-0002-4055-8442 ; artis.kons@lu.lv

Liāna Orola : 0000-0001-6069-7813 ; liana.orola@lu.lv

Anatoly Mishnev : 0000-0001-9905-3257 ; mishnevs@osi.lv

Dmitrijs Stepanovs : d_stepanovs@osi.lv

Liliana Mazur : 0000-0001-8283-3484 ; liliana.mazur@mail.umcs.pl

Magdalena Skiba: magdalena.skiba@onet.pl

Marta K. Dudek : 0000-0003-3412-0177 ; mdudek@cbmm.lodz.pl

Nicolas Fantozzi : 0000-0002-4561-8344 ; nicolas.fantozzi@enscm.fr

David Virieux : 0000-0002-6495-9478 ; david.virieux@enscm.fr

Evelina Colacino : 0000-0002-1179-4913 ; evelina.colacino@umontpellier.fr

Agris Bērziņš: 0000-0002-4149-8971 ; agris.berzins@lu.lv

ACKNOWLEDGMENT

The crystal structure prediction work was carried out at UCL in the laboratory of Prof. Sally Price using CSP computational infrastructure developed under EPSRC EP/K039229/1.

A.B., A.K, A.T.D. thank Profs Adjiman and Pantelides (Imperial College) for use of CrystalPredictor and CrystalOptimizer, Prof. Sally Price and Dr Louise Price for introduction with background and practical aspects of crystal structure prediction.

M.K.D. acknowledges financial support from Polish National Science Centre under Sonata grant No. UMO-2018/31/D/ST4/01995, as well as from PL-GRID infrastructure.

E.C. expresses her gratitude towards BetaInnov (www.beta-innov.com) for providing the planetary milling equipment for conducting the synthesis of dantrolene. E.C., N.F. and D.V. are grateful to Région Occitanie (France) for the Pre-Maturation 2020 – MECH-API grant (ESR_PRE-MAT – 00262).

This article is based upon work from COST Action CA18112 Mechanochemistry for Sustainable Industry, [77,77] supported by COST (European Cooperation in Science and Technology).
COST (European Cooperation in Science and Technology) is a funding agency for research and innovation networks. Our Actions help connect research initiatives across Europe and enable scientists to grow their ideas by sharing them with their peers. This boosts their research, career and innovation. www.cost.eu

REFERENCES

(1) Cruz-Cabeza, A. J.; Reutzel-Edens, S. M.; Bernstein, J. Facts and Fictions about Polymorphism. *Chem. Soc. Rev.* 2015, *44* (23), 8619–8635. https://doi.org/10.1039/C5CS00227C.

(2) Werner, J. E.; Swift, J. A. Organic Solvates in the Cambridge Structural Database. *CrystEngComm* 2021, *23* (7), 1555–1565. https://doi.org/10.1039/D0CE01749C.

(3) Wawrzycka-Gorczyca, I.; Borowski, P.; Osypiuk-Tomasik, J.; Mazur, L.; Koziol, A. E. Crystal Structure of Olanzapine and Its Solvates. Part 3. Two and Three-Component Solvates with Water, Ethanol, Butan-2-Ol and Dichloromethane. *J. Mol. Struct.* 2007, *830* (1–3), 188–197. https://doi.org/10.1016/J.MOLSTRUC.2006.07.017.

(4) Bhardwaj, R. M.; McMahon, J. A.; Nyman, J.; Price, L. S.; Konar, S.; Oswald, I. D. H.; Pulham, C. R.; Price, S. L.; Reutzel-Edens, S. M. A Prolific Solvate Former, Galunisertib, under the Pressure of Crystal Structure Prediction, Produces Ten Diverse Polymorphs. *J. Am. Chem. Soc.* 2019, *141* (35), 13887–13897. https://doi.org/10.1021/jacs.9b06634.

(5) Qu, H.; Zhang, J.; Zhang, G.; Li, Z.; Liu, Y.; Wu, S.; Gong, J. Structural Insights into the Highly Solvating System of Axitinib via Binary and Ternary Solvates. *Cryst. Growth Des.* 2022, *22* (2), 1083–1093. https://doi.org/10.1021/acs.cgd.1c01021.

(6) Bingham, A. L.; Hughes, D. S.; Hursthouse, M. B.; Lancaster, R. W.; Tavener, S.; Threlfall, T. L. Over One Hundred Solvates of Sulfathiazole. *Chem. Commun.* 2001, No. 7, 603–604. https://doi.org/10.1039/B009540K.

(7) Eszter, T.; Violetta, K.; György, P.; Zoltán, F.; Jan, R.; Eliška, S.; Michal, D. Rationalization of the Formation and Stability of Bosutinib Solvated Forms. *CrystEngComm* 2016, *18* (48), 9260–9274. https://doi.org/10.1039/C6CE01834C.

(8) Sarma, B.; Sanphui, P.; Nangia, A. Polymorphism in Isomeric Dihydroxybenzoic Acids. *Cryst. Growth Des.* 2010, *10* (5), 2388–2399. https://doi.org/10.1021/CG100220z.
(9) Varughese, S.; Desiraju, G. R. Using Water as a Design Element in Crystal Engineering. Host-Guest Compounds of Hydrated 3,5-Dihydroxybenzoic Acid. *Cryst. Growth Des.* 2010, *10* (9), 4184–4196. https://doi.org/10.1021/CG100872W.
(10) Steed, J. W. The Role of Co-Crystals in Pharmaceutical Design. *Trends Pharmacol. Sci.* 2013, *34* (3), 185–193. https://doi.org/10.1016/J.TIPS.2012.12.003.
(11) Kallay, E.; Kutner, A.; Braga, D.; Casali, L.; Grepioni, F. The Relevance of Crystal Forms in the Pharmaceutical Field: Sword of Damocles or Innovation Tools? *Int. J. Mol. Sci.* 2022, *23* (16), 9013. https://doi.org/10.3390/IJMS23169013.
(12) Beckmann, W. 10. Solubility and Phase Behaviour from a Drug Substance Manufacturing Perspective. *Solubility Pharm. Chem.* 2019, 259–318. https://doi.org/10.1515/9783110559835-010/HTML.
(13) Griesser, U. J. The Importance of Solvates. *Polymorph. Pharm. Ind.* 2006, 211–233. https://doi.org/10.1002/3527607889.CH8.
(14) Boothroyd, S.; Kerridge, A.; Broo, A.; Buttar, D.; Anwar, J. Why Do Some Molecules Form Hydrates or Solvates? *Cryst. Growth Des.* 2018, *18* (3), 1903–1908. https://doi.org/10.1021/acs.cgd.8b00160.
(15) Braun, D. E.; Griesser, U. J. Why Do Hydrates (Solvates) Form in Small Neutral Organic Molecules? Exploring the Crystal Form Landscapes of the Alkaloids Brucine and Strychnine. *Cryst. Growth Des.* 2016, *16* (11), 6405–6418. https://doi.org/10.1021/acs.cgd.6b01078.
(16) Qi, L.; Jin, Y.; Li, H.; Dong, Y.; Xie, C. The Role of Solvent in Tautomer Solvate Crystallization: A Case of 6-Amino-1,3-Dimethyl-5-Nitrosouracil. *Trans. Tianjin Univ.* 2020, *26* (6), 458–469. https://doi.org/10.1007/s12209-020-00247-7.
(17) Zhang, F.; Wang, L.; Fang, W.; Liu, Y.; Shi, P.; Liang, P.; Gao, Z.; Bao, Y. Understanding the Role of Solvent Polarity in the Molecular Self-Assembly Process of Etoricoxib Solvates. *Cryst. Growth Des.* 2020, *20* (6), 3650–3662. https://doi.org/10.1021/acs.cgd.9b01399.
(18) Price, C. P.; Glick, G. D.; Matzger, A. J. Dissecting the Behavior of a Promiscuous Solvate Former. *Angew. Chemie - Int. Ed.* 2006, *45* (13), 2062–2066. https://doi.org/10.1002/anie.200503533.
(19) Bērziņš, A.; Actiņš, A. Why Do Chemically Similar Pharmaceutical Molecules Crystallize in Different Structures: A Case of Droperidol and Benperidol. *Cryst. Growth Des.* 2016, *16* (3), 1643–1653. https://doi.org/10.1021/acs.cgd.5b01736.
(20) Trimdale, A.; Mishnev, A.; Bērziņš, A. Combined Use of Structure Analysis, Studies of Molecular Association in Solution, and Molecular Modelling to Understand the Different Propensities of Dihydroxybenzoic Acids to Form Solid Phases. *Pharmaceutics* 2021, *13* (5), 734. https://doi.org/10.3390/PHARMACEUTICS13050734/S1.
(21) Bērziņš, A.; Zvaniņa, D.; Trimdale, A. Detailed Analysis of Packing Efficiency Allows Rationalization of Solvate Formation Propensity for Selected Structurally Similar Organic Molecules. *Cryst. Growth Des.* 2018, *18* (4), 2040–2045. https://doi.org/10.1021/acs.cgd.7b01457.
(22) Konnert, L.; Lamaty, F.; Martinez, J.; Colacino, E. Recent Advances in the Synthesis of Hydantoins: The State of the Art of a Valuable Scaffold. *Chem. Rev.* 2017, *117* (23), 13757–13809. https://doi.org/10.1021/ACS.CHEMREV.7B00067.
(23) Colacino, E.; Porcheddu, A.; Charnay, C.; Delogu, F. From Enabling Technologies to Medicinal Mechanochemistry: An Eco-Friendly Access to Hydantoin-Based Active Pharmaceutical Ingredients. *React. Chem. Eng.* 2019, *4* (7), 1179–1188. https://doi.org/10.1039/C9RE00069K.
(24) World Health Organization model list of essential medicines: 21st list 2019 https://apps.who.int/iris/handle/10665/325771 (accessed Sep 8, 2022).
(25) Krause, T.; Gerbershagen, M. U.; Fiege, M.; Weißhorn, R.; Wappler, F. Dantrolene--a Review of Its Pharmacology, Therapeutic Use and New Developments. *Anaesthesia* 2004, *59* (4), 364–373. https://doi.org/10.1111/J.1365-2044.2004.03658.X.
(26) Colacino, E.; Porcheddu, A.; Halasz, I.; Charnay, C.; Delogu, F.; Guerra, R.; Fullenwarth, J.

Mechanochemistry for "No Solvent, No Base" Preparation of Hydantoin-Based Active Pharmaceutical Ingredients: Nitrofurantoin and Dantrolene. *Green Chem*. 2018, *20* (13), 2973–2977. https://doi.org/10.1039/C8GC01345D.
(27) Altomare, A.; Cuocci, C.; Giacovazzo, C.; Moliterni, A.; Rizzi, R.; Corriero, N.; Falcicchio, A. EXPO2013: A Kit of Tools for Phasing Crystal Structures from Powder Data. *J. Appl. Cryst.* 2013, *46* (4), 1231–1235. https://doi.org/10.1107/S0021889813013113.
(28) Altomare, A.; Campi, G.; Cuocci, C.; Eriksson, L.; Giacovazzo, C.; Moliterni, A.; Rizzi, R.; Werner, P. E. Advances in Powder Diffraction Pattern Indexing: N-TREOR09. *J. Appl. Cryst.* 2009, *42* (5), 768–775. https://doi.org/10.1107/S0021889809025503.
(29) Boultif, A.; Louër, D. Powder Pattern Indexing with the Dichotomy Method. *J. Appl. Cryst.* 2004, *37* (5), 724–731. https://doi.org/10.1107/S0021889804014876.
(30) Le Bail, A.; Duroy, H.; Fourquet, J. L. Ab-Initio Structure Determination of LiSbWO6 by X-Ray Powder Diffraction. *Mater. Res. Bull.* 1988, *23* (3), 447–452. https://doi.org/10.1016/0025-5408(88)90019-0.
(31) Pienaar, E. W.; Caira, M. R.; Lötter, A. P. Polymorphs of Nitrofurantoin. 2. Preparation and X-Ray Crystal Structures of Two Anhydrous Forms of Nitrofurantoin. *J. Crystallogr. Spectrosc. Res.* 1993, *23* (10), 785–790. https://doi.org/10.1007/BF01247241.
(32) Tanaka, R.; Akimoto, T.; Haramura, M.; Tanaka, A.; Hirayama, N. Structure of Dantrolene. *Anal. Sci. X-ray Struct. Anal. Online* 2004, *20* (3), x97–x98. https://doi.org/10.2116/ANALSCIX.20.X97.
(33) Coelho, A. A.; Kern, A.; IUCr. Indexing of Powder Diffraction Patterns by Iterative Use of Singular Value Decomposition. *Acta Cryst.* 2002, *58* (s1), 227–227. https://doi.org/10.1107/S0108767302094102.
(34) Sheldrick, G. M.; IUCr. Crystal Structure Refinement with SHELXL. *Acta Cryst.* 2015, *71* (1), 3–8. https://doi.org/10.1107/S2053229614024218.
(35) Sheldrick, G. M. SHELXS-97 and SHELXL-97, Program for Crystal Structure Solution and Refinement. *Univ. Göttingen* 1997.
(36) CrysAlisPRO Software System. *Rigaku Oxford Diffr.* 2019.
(37) Farrugia, L. J.; IUCr. WinGX Suite for Small-Molecule Single-Crystal Crystallography. *J. Appl. Cryst.* 1999, *32* (4), 837–838. https://doi.org/10.1107/S0021889899006020.
(38) Frisch, M. J.; Trucks, G. W.; Schlegel, H. B.; Scuseria, G. E. .; Robb, M. A.; Cheeseman, J. R.; Scalmani, G.; Barone, V. . M.; B.; Petersson, G. A.; Nakatsuji, H.; Caricato, M.; Li, X.; Hratchian, H.; P.; Izmaylov, A. F.; Bloino, J.; Zheng, G.; Sonnenberg, J. L.; Hada, M. .; Ehara, M.; Toyota, K.; Fukuda, R.; Hasegawa, J.; Ishida, M. .; Nakajima, T.; Honda, Y.; Kitao, O.; Nakai, H.; Vreven, T. .; Montgomery, J. A., Jr.; Peralta, J. E.; Ogliaro, F.; Bearpark, M. .; Heyd, J. J.; Brothers, E.; Kudin, K. N.; Staroverov, V. N. . K.; R.; Normand, J.; Raghavachari, K.; Rendell, A.; Burant, J. C. . I.; S. S.; Tomasi, J.; Cossi, M.; Rega, N.; Millam, J. M.; Klene, M. . K.; J. E.; Cross, J. B.; Bakken, V.; Adamo, C.; Jaramillo, J.; Gomperts, R. .; Stratmann, R. E.; Yazyev, O.; Austin, A. J.; Cammi, R.; Pomelli, C. .; Ochterski, J. W.; Martin, R. L.; Morokuma, K.; Zakrzewski, V. G. .; Voth, G. A.; Salvador, P.; Dannenberg, J. J.; Dapprich, S.; Daniels, A.; D.; Farkas, O.; Foresman, J. B.; Ortiz, J. V.; Cioslowski, J.; Fox, D. J. *Gaussian 09W Reference, Revision D.01*; Gaussian, Inc., Wallingford CT, 2016.
(39) Di Tommaso, D. The Molecular Self-Association of Carboxylic Acids in Solution: Testing the Validity of the Link Hypothesis Using a Quantum Mechanical Continuum Solvation Approach. *CrystEngComm* 2013, *15* (33), 6564–6577. https://doi.org/10.1039/c3ce40539g.
(40) Lu, T.; Chen, F. Multiwfn: A Multifunctional Wavefunction Analyzer. *J. Comput. Chem.* 2012, *33* (5), 580–592. https://doi.org/10.1002/jcc.22885.
(41) Humphrey, W.; Dalke, A.; Schulten, K. VMD: Visual Molecular Dynamics. *J. Mol. Graph.* 1996, *14* (1), 33–38. https://doi.org/10.1016/0263-7855(96)00018-5.
(42) Giannozzi, P.; Baroni, S.; Bonini, N.; Calandra, M.; Car, R.; Cavazzoni, C.; Ceresoli, D.; Chiarotti, G. L.; Cococcioni, M.; Dabo, I.; Dal Corso, A.; De Gironcoli, S.; Fabris, S.; Fratesi, G.; Gebauer, R.; Gerstmann, U.; Gougoussis, C.; Kokalj, A.; Lazzeri, M.; Martin-Samos, L.; Marzari,

N.; Mauri, F.; Mazzarello, R.; Paolini, S.; Pasquarello, A.; Paulatto, L.; Sbraccia, C.; Scandolo, S.; Sclauzero, G.; Seitsonen, A. P.; Smogunov, A.; Umari, P.; Wentzcovitch, R. M. QUANTUM ESPRESSO: A Modular and Open-Source Software Project for Quantum of Materials. *J. Phys. Condens. Matter* 2009, *21* (39), 395502. https://doi.org/10.1088/0953-8984/21/39/395502.

(43) Grimme, S. Semiempirical GGA-Type Density Functional Constructed with a Long-Range Dispersion Correction. *J. Comput. Chem.* 2006, *27* (15), 1787–1799. https://doi.org/10.1002/JCC.20495.

(44) Lund, A. M.; Orendt, A. M.; Pagola, G. I.; Ferraro, M. B.; Facelli, J. C. Optimization of Crystal Structures of Archetypical Pharmaceutical Compounds: A Plane-Wave DFT-D Study Using Quantum Espresso. *Cryst. Growth Des.* 2013, *13* (5), 2181–2189. https://doi.org/10.1021/CG4002797.

(45) Spek, A. L. Structure Validation in Chemical Crystallography. *Acta Crystallogr. Sect. D Biol. Crystallogr.* 2009, *65* (2), 148–155. https://doi.org/10.1107/S090744490804362X.

(46) MacRae, C. F.; Sovago, I.; Cottrell, S. J.; Galek, P. T. A.; McCabe, P.; Pidcock, E.; Platings, M.; Shields, G. P.; Stevens, J. S.; Towler, M.; Wood, P. A. Mercury 4.0: From Visualization to Analysis, Design and Prediction. *J. Appl. Crystallogr.* 2020, *53* (1), 226–235. https://doi.org/10.1107/S1600576719014092.

(47) Mackenzie, C. F.; Spackman, P. R.; Jayatilaka, D.; Spackman, M. A. CrystalExplorer Model Energies and Energy Frameworks: Extension to Metal Coordination Compounds, Organic Salts, Solvates and Open-Shell Systems. *IUCrJ* 2017, *4* (5), 575–587. https://doi.org/10.1107/S205225251700848X.

(48) Karamertzanis, P. G.; Pantelides, C. C. Ab Initio Crystal Structure Prediction. II. Flexible Molecules. *Mol. Phys.* 2010, *105* (2–3), 273–291. https://doi.org/10.1080/00268970601143317.

(49) Coombes, D. S.; Price, S. L.; Willock, D. J.; Leslie, M. Role of Electrostatic Interactions in Determining the Crystal Structures of Polar Organic Molecules. A Distributed Multipole Study. *J. Phys. Chem.* 1996, *100* (18), 7352–7360. https://doi.org/10.1021/JP960333B.

(50) Price, S. L.; Leslie, M.; Welch, G. W. A.; Habgood, M.; Price, L. S.; Karamertzanis, P. G.; Day, G. M. Modelling Organic Crystal Structures Using Distributed Multipole and Polarizability-Based Model Intermolecular Potentials. *Phys. Chem. Chem. Phys.* 2010, *12* (30), 8478–8490. https://doi.org/10.1039/C004164E/.

(51) Stone, A. J. Distributed Multipole Analysis: Stability for Large Basis Sets. *J. Chem. Theory Comput.* 2005, *1* (6), 1128–1132. https://doi.org/10.1021/ct050190+.

(52) Kazantsev, A. V.; Karamertzanis, P. G.; Adjiman, C. S.; Pantelides, C. C. Efficient Handling of Molecular Flexibility in Lattice Energy Minimization of Organic Crystals. *J. Chem. Theory Comput.* 2011, *7* (6), 1998–2016. https://doi.org/10.1021/CT100597E.

(53) Kons, A.; Mishnev, A.; Mukhametzyanov, T. A.; Buzyurov, A. V.; Lapuk, S. E.; Bērziņš, A. Hexamorphism of Dantrolene: Insight into the Crystal Structures, Stability, and Phase Transformations. *Cryst. Growth Des.* 2021, *21* (2), 1190–1201. https://doi.org/10.1021/acs.cgd.0c01508.

(54) Dudek, M. K.; Paluch, P.; Pindelska, E. Crystal Structures of Two Furazidin Polymorphs Revealed by a Joint Effort of Crystal Structure Prediction and NMR Crystallography. *Acta Crystallogr. Sect. B Struct. Sci. Cryst. Eng. Mater.* 2020, *76* (3), 322–335. https://doi.org/10.1107/S205252062000373X.

(55) Pienaar, E. W.; Caira, M. R.; Lötter, A. P. Polymorphs of Nitrofurantoin. I. Preparation and X-Ray Crystal Structures of Two Monohydrated Forms of Nitrofurantoin. *J. Crystallogr. Spectrosc. Res.* 1993, *23* (9), 739–744. https://doi.org/10.1007/BF01187276.

(56) Tutughamiarso, M.; Bolte, M.; Wagner, G.; Egert, E. Five Pseudopolymorphs and a Cocrystal of Nitrofurantoin. *Acta Crystallogr. Sect. C Cryst. Struct. Commun.* 2011, *67* (1), o18–o25. https://doi.org/10.1107/S0108270110046755.

(57) Cvetkovski, A.; Ferretti, V. Crystal Structure and Packing Analysis of Nitrofurantoin N,N-Dimethylformamide Solvate. *Crystallogr. Reports* 2016, *61* (4), 611–615. https://doi.org/10.1134/S1063774516040040.

(58) Vangala, V. R.; Chow, P. S.; Tan, R. B. H. Nitrofurantoin Methanol Monosolvate. *Acta Crystallogr. Sect. E Struct. Reports Online* 2011, *67* (3), o550–o551. https://doi.org/10.1107/S1600536811003679.
(59) Orola, L.; Mishnev, A.; Stepanovs, D.; Bērziņš., A. Crystallographic Study of Solvates and Solvate Hydrates of an Antibacterial Furazidin. https://doi.org/10.26434/chemrxiv-2022-rb0xk.
(60) Bērziņš, K.; Kons, A.; Grante, I.; Dzabijeva, D.; Nakurte, I.; Actiņš, A. Multi-Technique Approach for Qualitative and Quantitative Characterization of Furazidin Degradation Kinetics under Alkaline Conditions. *J. Pharm. Biomed. Anal.* 2016, *129*, 433–440. https://doi.org/10.1016/J.JPBA.2016.07.039.
(61) Habgood, M.; Price, S. L.; Portalone, G.; Irrera, S. Testing a Variety of Electronic-Structure-Based Methods for the Relative Energies of 5-Formyluracil Crystals. *J. Chem. Theory Comput.* 2011, *7* (9), 2685–2688. https://doi.org/10.1021/CT200354T.
(62) Caira, M. R.; Pienaar, E. W.; Lötter, A. P. Polymorphism and Pseudopolymorphism of the Antibacterial Nitrofurantoin. *Mol. Cryst. Liq. Cryst. Sci. Technol. Sect. A. Mol. Cryst. Liq. Cryst.* 2006, *278–279*, 241–264. https://doi.org/10.1080/10587259608042194.
(63) Kelly, R. C. A Molecular Approach to Understanding the Directed Nucleation and Phase Transformation of Carbamazepine and Nitrofurantoin in Aqueous and Organic Solutions., University of Michigan, 2003.
(64) Bērziņš., A.; Trimdale-Deksne, A.; Belyakov, S.; ter Horst, J. H. Reversing the Polymorphic Outcome of Crystallization and the Apparent Relative Stability of Nitrofurantoin Polymorphs Using Additives. Manuscript in Preparation.
(65) Vangala, V. R.; Chow, P. S.; Tan, R. B. H. Co-Crystals and Co-Crystal Hydrates of the Antibiotic Nitrofurantoin: Structural Studies and Physicochemical Properties. *Cryst. Growth Des.* 2012, *12* (12), 5925–5938. https://doi.org/10.1021/CG300887P.
(66) Tian, F.; Baldursdottir, S.; Rantanen, J. Effects of Polymer Additives on the Crystallization of Hydrates: A Molecular-Level Modulation. *Mol. Pharm.* 2009, *6* (1), 202–210. https://doi.org/10.1021/MP800142Z.
(67) Tian, F.; Qu, H.; Louhi-Kultanen, M.; Rantanen, J. Mechanistic Insight into the Evaporative Crystallization of Two Polymorphs of Nitrofurantoin Monohydrate. *J. Cryst. Growth* 2009, *311* (8), 2580–2589. https://doi.org/10.1016/J.JCRYSGRO.2009.02.004.
(68) Tian, F.; Qu, H.; Louhi-Kultanen, M.; Rantanen, J. Insight into Crystallization Mechanisms of Polymorphic Hydrate Systems. *Chem. Eng. Technol.* 2010, *33* (5), 833–838. https://doi.org/10.1002/CEAT.200900572.
(69) Boetker, J. P.; Rantanen, J.; Arnfast, L.; Doreth, M.; Raijada, D.; Loebmann, K.; Madsen, C.; Khan, J.; Rades, T.; Müllertz, A.; Hawley, A.; Thomas, D.; Boyd, B. J. Anhydrate to Hydrate Solid-State Transformations of Carbamazepine and Nitrofurantoin in Biorelevant Media Studied in Situ Using Time-Resolved Synchrotron X-Ray Diffraction. *Eur. J. Pharm. Biopharm.* 2016, *100*, 119–127. https://doi.org/10.1016/J.EJPB.2016.01.004.
(70) Trimdale, A.; Bērziņš, A. Evaluation of Aspects Controlling Crystallization of Nitrofurantoin. *Key Eng. Mater.* 2019, *800*, 9–13. https://doi.org/10.4028/www.scientific.net/KEM.800.9.
(71) Price, S. L. Why Don't We Find More Polymorphs? *Acta Crystallogr. Sect. B Struct. Sci. Cryst. Eng. Mater.* 2013, *69* (4), 313–328. https://doi.org/10.1107/S2052519213018861.
(72) Price, S. L. Is Zeroth Order Crystal Structure Prediction (CSP_0) Coming to Maturity? What Should We Aim for in an Ideal Crystal Structure Prediction Code? *Faraday Discuss.* 2018, *211* (0), 9–30. https://doi.org/10.1039/C8FD00121A.
(73) Braun, D. E.; McMahon, J. A.; Bhardwaj, R. M.; Nyman, J.; Neumann, M. A.; Van De Streek, J.; Reutzel-Edens, S. M. Inconvenient Truths about Solid Form Landscapes Revealed in the Polymorphs and Hydrates of Gandotinib. *Cryst. Growth Des.* 2019, *19* (5), 2947–2962. https://doi.org/10.1021/ACS.CGD.9B00162.
(74) Beran, G. J. O.; Sugden, I. J.; Greenwell, C.; Bowskill, D. H.; Pantelides, C. C.; Adjiman, C. S. How Many More Polymorphs of ROY Remain Undiscovered. *Chem. Sci.* 2022, *13* (5), 1288–1297. https://doi.org/10.1039/D1SC06074K.

(75) Anderson, M. W.; Bennett, M.; Cedeno, R.; Cölfen, H.; Cox, S. J.; Cruz-Cabeza, A. J.; Yoreo, J. J. De; Drummond-Brydson, R.; Dudek, M. K.; Fichthorn, K. A.; Finney, A. R.; Ford, I.; Galloway, J. M.; Gebauer, D.; Grossier, R.; Harding, J. H.; Hare, A.; Horváth, D.; Hunter, L.; Kim, J.; Kimura, Y.; Kirschhock, C. E. A.; Kiselev, A. A.; Kras, W.; Kuttner, C.; Lee, A. Y.; Liao, Z.; Maini, L.; Lill, S. O. N.; Pellens, N.; Price, S. L.; Rietveld, I. B.; Rimer, J. D.; Roberts, K. J.; Rogal, J.; Salvalaglio, M.; Sandei, I.; Schuszter, G.; Sefcik, J.; Sun, W.; Horst, J. H. ter; Ukrainczyk, M.; Driessche, A. E. S. Van; Veesler, S.; Vekilov, P. G.; Verma, V.; Whale, T.; Wheatcroft, H. P.; Zeglinski, J. Understanding Crystal Nucleation Mechanisms: Where Do We Stand? General Discussion. *Faraday Discuss*. 2022, *235* (0), 219–272. https://doi.org/10.1039/D2FD90021A.

(76) Cedeno, R.; Cruz-Cabeza, A.; Drummond-Brydson, R.; Dudek, M. K.; Edkins, K.; Fichthorn, K.; Finney, A. R.; Ford, I.; Galloway, J. M.; Grossier, R.; Kim, J.; Kuttner, C.; Maini, L.; Meldrum, F.; Miller, M.; Morris, P.; Lill, S. O. N.; Pokroy, B.; Price, S.; Rietveld, I. B.; Rimer, J.; Roberts, K.; Rogal, J.; Salvalaglio, M.; Sefcik, J.; Sun, W.; Veesler, S.; Vekilov, P.; Wheatcroft, H.; Whittaker, M.; Zhao, R. Controlling Polymorphism: General Discussion. *Faraday Discuss*. 2022, *235* (0), 508–535. https://doi.org/10.1039/D2FD90023H.

(77) Hernández, J. G.; Halasz, I.; Crawford, D. E.; Krupicka, M.; Baláž, M.; André, V.; Vella-Zarb, L.; Niidu, A.; García, F.; Maini, L.; Colacino, E. European Research in Focus: Mechanochemistry for Sustainable Industry (COST Action MechSustInd). *European J. Org. Chem*. 2020, *2020* (1), 8–9. https://doi.org/10.1002/EJOC.201901718.

(77) For more information on COST Action CA18112 'Mechanochemistry for Sustainable Industry' : http://www.mechsustind.eu/ (accessed May 21, 2022).

For Table of Contents Use Only

Crystallographic and Computational Analysis of Solid Form Landscape of Three Structurally Related Imidazolidine-2,4-dione Active Pharmaceutical Ingredients: Nitrofurantoin, Furazidin and Dantrolene

*Aija Trimdale-Deksne, Artis Kons, Liāna Orola, Anatoly Mishnev, Dmitrijs Stepanovs, Liliana Mazur, Magdalena Skiba, Marta K. Dudek, Nicolas Fantozzi, David Virieux, Evelina Colacino, Agris Bērziņš**